SABA Publishing

Journal of Mathematical Analysis and Modeling
jmam.sabapub.com
ISSN 2709-5924

J Math Anal & Model
(2026)7(1) : 1-31
doi:10.48185/jmam.v7i1.1915

MATHEMATICAL MODEL FOR THE DYNAMICS OF COVID-19 AND MONKEYPOX CO-INFECTION CONSIDERING THE EFFECTS OF VACCINATION, QUARANTINE, AND REINFECTION

FRANKLINE C. EZE [a], MARTIN C. OBI[b], NNEKA O. IHEONU[b], NNAMDI N. ARAKA[b] EMEKA C. GODWIN [b]

[a] Department of Mathematics and Statistics, Federal Polytechnic Nekede, Owerri, Nigeria
[b] Department of Mathematics, Federal University of Technology, Owerri, Nigeria

• *Received: 14 December 2025* • *Accepted: 15 March 2026* • *Published Online: 28 April 2026*

Abstract

This study presents a deterministic compartmental model for the co-infection dynamics of COVID-19 and Monkeypox, incorporating vaccination, quarantine, treatment, and reinfection. The model is shown to be mathematically well-posed, and the disease-free equilibrium (DFE) and the basic reproduction number R_0 are derived. The local and global stability of the DFE are established using the next-generation matrix and the Castillo–Chavez and Song method, while the global stability of the endemic equilibrium is proven using a Lyapunov function. A modification parameter $\eta \in [0,1]$, representing treatment effectiveness in reducing disease-induced mortality, is investigated. Numerical simulations show that effective treatment (low η) reduces mortality but increases the long-term treatment population, whereas ineffective treatment (high η) leads to higher mortality among treated individuals. The results also indicate that COVID-19 enhances Monkeypox transmission through increased co-infections. Overall, the study highlights the importance of integrated strategies involving vaccination, quarantine, and effective treatment to control the co-infection of COVID-19 and Monkeypox.

Keywords: COVID-19; Monkeypox; Co-infection dynamics; Vaccination; Lyapunov functions; Mortality reduction.

1. Introduction

COVID-19 was first reported in Wuhan, China, in December 2019. Due to its rapid global transmission and the severity of symptoms, it was declared a Public Health Emergency of International Concern on January 30, 2020, and subsequently a pandemic on March 11, 2020. The pandemic disrupted all sectors, including healthcare, the economy, education, travel, and day-to-day activities, which highlighted that pandemic preparedness has major loopholes. COVID-19 also falls under the Coronaviridae family, which

*Corresponding author: ezefrankline@imsuonline.edu.ng

uses ACE2 receptors to enter host cells [1]. There are indications that COVID-19 has a natural reservoir in bats, but it can also be transmitted by pangolins [2, 32, 19]. Such zoonosis can also be attributed to increasing interactions between human healthcare and nature itself. Transmission of COVID-19 occurs between people via respiratory droplets, especially in environments with insufficient ventilation, as well as through contact with contaminated surfaces. The higher transmission rate compared to SARS-CoV-1 (initial coronavirus) contributed to a quick increase in infection cases. Initial estimates of the basic reproduction number (R_0) were between 2 and 3. [4, 34, 15, 25]. The range of the disease's severity has been immense. Seniors and those with comorbid conditions (diabetes, hypertension, cardiovascular disease, immunosuppression) are at greater risk for complications like pneumonia, ARDS, organ failure, and mortality [5, 33, 31, 36]. While it was initially deemed a respiratory illness, it has been acknowledged that it has multisystem manifestations, including neurological, cardiovascular, nephrological, and hematological components. These range from respiratory manifestations of fever, cough, anosmia, and dyspnea to gastrointestinal symptoms [6, 37]. The diagnostic test primarily employed for confirming an infection is reverse transcription polymerase chain reaction, with rapid tests for antigens and antibodies being used despite their lack of accuracy. Delays in testing, availability, and lack of resources were some of the key factors. To manage transmission, governments implemented Non-Pharmaceutical Interventions, including lockdowns, curfews, physical distancing, school closures, and the use of face masks, which incurred significant economic and social costs. The development of vaccines completely changed how a pandemic like COVID-19 can be treated effectively, with mRNA vaccines like Pfizer-BioNTech and Moderna, as well as vector-based vaccines like AstraZeneca, showing substantial decreases in symptoms. The COVID-19 pandemic brought a plethora of weaknesses in the world's healthcare systems to the fore, re-emphasizing the importance of a sturdy surveillance system, effective Non-Pharmaceutical Interventions, equitable access to vaccines, and constant preparation for a

Monkeypox is a re-emerging zoonotic infection caused by simian monkey viruses referred to as Monkeypox viruses. These viruses belong to the Orthopoxvirus family, which is closely related to variola viruses that cause smallpox. Monkeypox was identified as a monkey infection in 1958 and as a human infection in 1970 in the Democratic Republic of Congo, as reported in a 1972 study by [7]. The significant resurgence of monkeypox occurred in 2022 when reports indicated human-to-human transmission in various non-endemic countries, raising global concerns, as noted by the WHO in that year. A factor that has increased vulnerability to this re-emergence of monkeypox has been waning immunity among humans due to smallpox eradication, as reported. There are two clades of MPXV, with a severe form in Central Africa and a usually milder form in West Africa, which was responsible for the 2022 outbreak [8]. Transmission can occur through contact with infected animals, individuals, and contaminated materials. Zoonotic transmission is associated with bites, bodily fluids, and undercooked bushmeat. Although human-to-human transmission is less efficient, it can occur through respiratory droplets, skin lesions, and contaminated objects. The 2022 outbreak revealed a new trend characterized by prolonged transmission among close contacts. Clinical manifestations of monkeypox are fever, fatigue, lymphadenopathy, and then a distinctive rash that develops from macules to pustules [10]. Atypical cases, particularly in the genital area, resulted in misinterpreta-

tions of the illness in the 2022 outbreak, highlighting a lack of understanding with regards to this. This can only be determined by PCR reaction test results. Historically restricted to African forest ecosystems, Monkeypox has been seen in a number of worldwide outbreaks, including a 2003 outbreak in the U.S. that was associated with imported domestic pets, as well as travel-related cases from 2018-2019 [11]. This 2022 worldwide increase represents a huge epidemiological transition, which has sparked concerns over potential evolutions of this virus as well as preparedness worldwide, as reported by [12]. The World Health Organization has declared it a Public Health Emergency of International Concern in July 2022. “Methods of control are aimed at early detection, isolation of cases, tracing contacts, vaccination, and public education.” Smallpox vaccines like ACAM2000 and MVA-BN/JYNNEOS provide cross-protection due to their antigen-related characteristics. Effective communication plays a significant role in overcoming stigmatization, as “risk of infection does not discriminate among demographics.” An important lesson learned from the COVID-19 pandemic has been improvement in preparedness through enhanced global surveillance and response capabilities. The monkeypox outbreak that occurred in Africa has highlighted its potential as a long-term challenge for public health. There are many issues that must be addressed in order to effectively manage monkeypox.

Co-infection with COVID-19 and Monkeypox virus (MPXV) represents a rising challenge for worldwide healthcare. "COVID-19 has been a constant cause of morbidity and mortality since 2019, with Monkeypox cases, which were restricted to Africa until 2022, spreading to other continents that year as well." [13]. There are now cases of infections with both viruses being reported in various areas, especially in immunocompromised patients. This represents a challenge due to increased cases of complications from co-infections, which also put extra stress on healthcare systems. These two viruses present common symptoms that include fever, weakness, and respiratory manifestations, which make it extremely challenging to identify and confirm diagnoses clinically and in laboratories, especially in developing countries [14]. There has been no insight into their biological interactions, even though immune dysfunction caused by COVID-19 could increase vulnerability to the MPXV infection, and the cytokine storm initiated by MPXV infection can prolong the severe courses of COVID-19 infection [16, 35]. Co-infection presents a challenge to public healthcare systems that are already strained in terms of diagnostic capabilities, isolation capacity, and staffing levels. Additionally, co-infection poses a challenge when it comes to vaccination strategies, as COVID-19 vaccines are mRNA/viral vector-based and protect against viruses from a different family, while Monkeypox vaccines are MVA-BN-based and target a completely different family of viruses. [17, 28]. The concurrent presence of both diseases highlights the impact of areas with high population density, transmission points, displaced individuals, and those with weakened immune systems, such as those with HIV/AIDS, who are also at risk of undetected co-infection [38]. Additionally, misconceptions surrounding both diseases can lead to delays in seeking care, as noted in a study by [18, 30, 31].

A mathematical model for co-infection of COVID-19 and Monkeypox has been developed in this thesis, which has been inspired by increasing evidence that suggests that when many pathogens co-circulate, their behaviors are not simply additive. The challenge now has been that both COVID-19 and Monkeypox are spreading simultaneously. Extending [20], this manuscript aims to enhance this already established mathematical

framework by including important biological components that were not accounted for in previous modeling structures. These additional components are: vaccination for both infections, vaccine failure, reinfection with COVID-19 modeled as a direct transition into the infectious class for those with dual infections, declining immunity among doubly infected individuals, and a transition between single infections and doubly infected. , The model equations are formulated as a set of nonlinear ordinary differential equations, and the expression for the basic reproduction number, R_O, has been derived using the Next-Generation Matrix method. The stability of both the disease-free and endemic equilibria has been proven. Sensitivity analyses utilizing Latin Hypercube Sampling indicate that a coordinated approach to vaccination, quarantine, and treatment strategies is essential. Finally, this work advances co-infection modeling by integrating practical epidemiological characteristics. The study directly addresses several gaps in existing research and strengthens the foundation for analyzing other co-circulating pathogens.

- Absence of vaccination for both COVID-19 and Monkeypox in existing co-infection models.
- Lack of incorporation of vaccination failure and imperfect vaccine protection.
- Insufficient representation of two-way transitions between single-infected and co-infected classes.
- Inadequate treatment of cross-disease interactions affecting transmission and progression.
- Scarcity of integrated intervention frameworks combining vaccination, quarantine, and treatment for both diseases.

2. Description of Model

This study develops a deterministic compartmental model for the transmission dynamics of COVID-19 and Monkeypox co-infection in human and rodent populations. The human population $N_h(t)$ is subdivided into twelve compartments:

$$S_h,\ V_c,\ V_m,\ E_c^h,\ E_m^h,\ Q_c,\ Q_m,\ I_c^h,\ I_m^h,\ I_{cm}^h,\ T_h,\ R_h,$$

while the rodent population $N_r(t)$ consists of:

$$S_r,\ E_r,\ I_r.$$

Humans and rodents are recruited at rates Λ_h and Λ_r. Vaccination against COVID-19 and Monkeypox occurs at rates θ_c and θ_m, with vaccine failure rates ψ_c and ψ_m. Human-to-human transmission occurs at rates β_c (COVID-19) and β_m (Monkeypox), rodent-to-human Monkeypox transmission at rate β_1, and rodent-to-rodent transmission at rate β_r.

Exposed humans progress to infectious classes at rates α_c^1 and α_m^1, or enter quarantine at rates α_c^2 and α_m^2. Exposed rodents progress to infection at rate α_r. Quarantined COVID-19 individuals recover naturally at rate σ, while Monkeypox has no natural recovery in quarantine. Symptomatic quarantined individuals move to treatment at rates ζ_c and ζ_m.

Infected individuals may enter treatment at rates γ_c and γ_m, or develop co-infection at rate π. Co-infected individuals enter treatment at rate γ_{cm} or recover from either disease at rates τ_m and τ_c. Treated individuals recover at rate ϕ. Natural mortality rates for humans and rodents are μ_h and μ_r, while disease-induced mortalities are δ_c, δ_m, and δ_{cm}. Mortality is reduced in treatment by modification parameter η.

Recovered individuals may be reinfected with COVID-19 at rates χ (post-recovery) and ω (due to waning immunity).

The forces of infection are given by:

$$\lambda_c(t) = \frac{\beta_c(I_c^h + I_{cm}^h)}{N_h}, \qquad \lambda_m(t) = \frac{\beta_1 I_r + \beta_m(I_m^h + I_{cm}^h)}{N_h}, \qquad \lambda_r(t) = \frac{\beta_r I_r}{N_r}.$$

The total population is:

$$N_h(t) = S_h + V_c + V_m + E_c^h + E_m^h + Q_c + Q_m + I_c^h + I_m^h + I_{cm}^h + T_h + R_h,$$

$$N_r(t) = S_r + E_r + I_r.$$

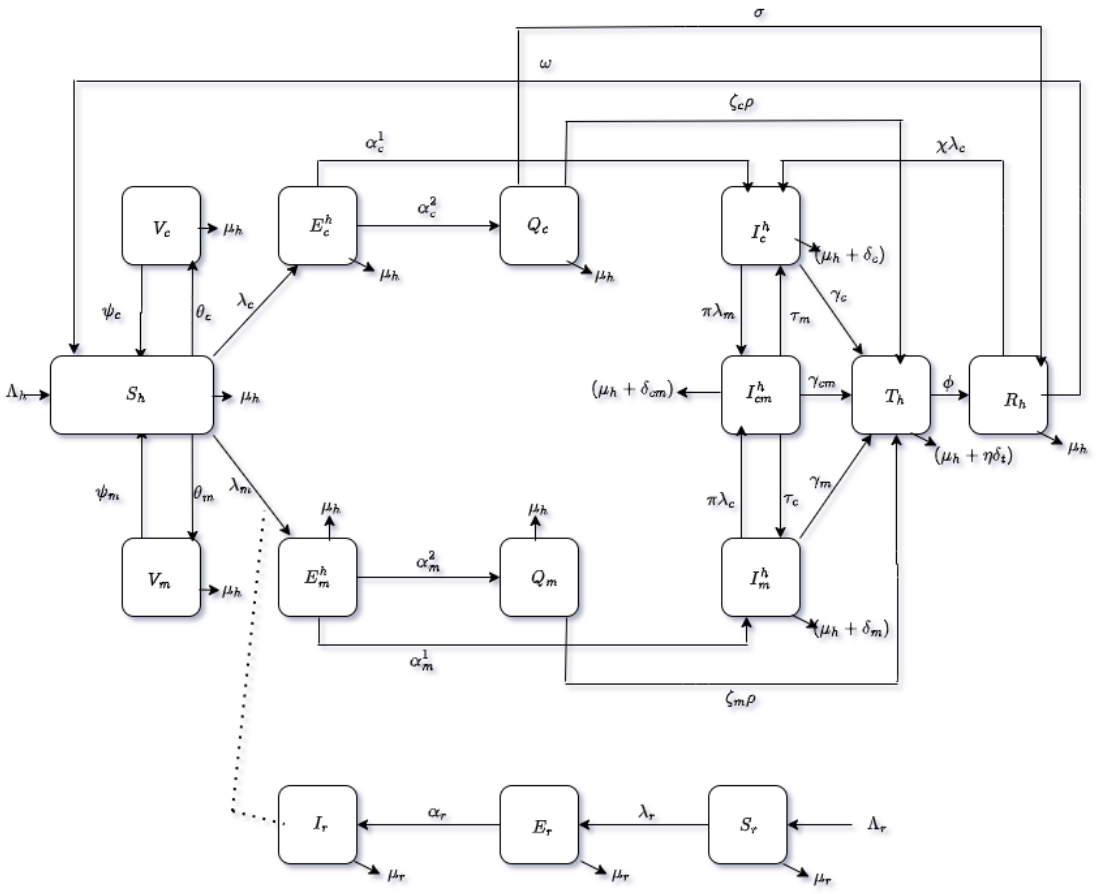

Figure 1: Schematic diagram of the model

2.1. Model Formulation

$$
\begin{aligned}
\frac{dS_h}{dt} &= \Lambda_h + \psi_c V_c + \psi_m V_m + \omega R_h - (\theta_c + \theta_m + \lambda_c + \lambda_m + \mu_h)\, S_h \\
\frac{dV_c}{dt} &= \theta_c S_h - (\psi_c + \mu_h) V_c \\
\frac{dV_m}{dt} &= \theta_m S_h - (\psi_m + \mu_h) V_m \\
\frac{dE_c^h}{dt} &= \lambda_c S_h - (\alpha_c^1 + \alpha_c^2 + \mu_h) E_c^h \\
\frac{dE_m^h}{dt} &= \lambda_m S_h - (\alpha_m^1 + \alpha_m^2 + \mu_h) E_m^h \\
\frac{dQ_c}{dt} &= \alpha_c^2 E_c^h - (\zeta_c \rho + \sigma + \mu_h) Q_c \\
\frac{dQ_m}{dt} &= \alpha_m^2 E_m^h - (\zeta_m \rho + \mu_h) Q_m \\
\frac{dI_c^h}{dt} &= \alpha_c^1 E_c^h + \chi \lambda_c R_h + \tau_m I_{cm}^h - (\pi \lambda_m + \gamma_c + \mu_h + \delta_c) I_c^h \\
\frac{dI_m^h}{dt} &= \alpha_m^1 E_m^h + \tau_c I_{cm}^h - (\pi \lambda_c + \gamma_m + \mu_h + \delta_m) I_m^h \\
\frac{dI_{cm}^h}{dt} &= \pi \lambda_m I_c^h + \pi \lambda_c I_m^h - (\tau_m + \tau_c + \gamma_{cm} + \mu_h + \delta_{cm}) I_{cm}^h \\
\frac{dT_h}{dt} &= \zeta_c \rho Q_c + \zeta_m \rho Q_m + \gamma_c I_c^h + \gamma_m I_m^h + \gamma_{cm} I_{cm}^h - (\phi + \mu_h + \eta \delta_t) T_h \\
\frac{dR_h}{dt} &= \phi T_h + \sigma Q_c - (\chi \lambda_c + \omega + \mu_h) R_h \\
\frac{dS_r}{dt} &= \Lambda_r - (\lambda_r + \mu_r) S_r \\
\frac{dE_r}{dt} &= \lambda_r S_r - (\alpha_r + \mu_r) E_r \\
\frac{dI_r}{dt} &= \alpha_r E_r - \mu_r I^r
\end{aligned}
\tag{2.1}
$$

where

$$
\begin{aligned}
\lambda_c(t) &= \frac{\beta_c (I_c^h + I_{cm}^h)}{N_h} \\
\lambda_m(t) &= \frac{\beta_1 I_r + \beta_m (I_m^h + I_{cm}^h)}{N_h}; \\
\lambda_r(t) &= \frac{\beta_r I_r}{N_r(t)}
\end{aligned}
$$

.

Table 1: Model parameters and description.

Parameter	**Description**
Λ_h	Recruitment rate for humans
Λ_r	Recruitment rate for rodents
β_c	Transmission rate of susceptible humans from infected COVID-19 humans
β_m	Transmission rate of susceptible humans from infected Monkeypox humans
β_r	Transmission rate of susceptible rodents from infected rodents
β_1	Transmission rate of susceptible humans from infected rodents
λ_c	Force of infection for COVID-19 infection
λ_m	Force of infection for Monkeypox infection
λ_r	Force of infection for rodents
α_c^1	Progression rate from exposed COVID-19 individuals to infectious COVID-19 humans
α_c^2	Progression rate from exposed COVID-19 individuals to quarantined COVID-19 humans
α_m^1	Progression rate from exposed Monkeypox individuals to infectious Monkeypox humans
α_m^2	Progression rate from exposed Monkeypox individuals to quarantined Monkeypox humans
α_r	Progression rate from exposed rodents to infectious rodents
θ_c	Vaccination rate for COVID-19
θ_m	Vaccination rate for Monkeypox
ψ_c	COVID-19 vaccine failure rate
ψ_m	Monkeypox vaccine failure rate
ζ_c	Treatment rate of quarantined COVID-19 individuals
ζ_m	Treatment rate of quarantined Monkeypox individuals
ρ	Rate of developing clinical symptoms during quarantine
τ_c	COVID-19 recovery rate for co-infected individuals
τ_m	Monkeypox recovery rate for co-infected individuals
π	Increased susceptibility to infection as a result of underlying sickness (COVID-19/Monkeypox)
σ	COVID-19 natural recovery rate
γ_c	Treatment rate of infected COVID-19 individuals
γ_m	Treatment rate of infected Monkeypox individuals
γ_{cm}	Treatment rate of co-infected COVID-19 and Monkeypox individuals
ϕ	Recovery rate of treated individuals
χ	Increased infectiousness of COVID-19 recovered individuals
δ_c	COVID-19 induced death rate
δ_m	Monkeypox induced death rate
δ_{cm}	Co-infected induced death rate
η	Modification parameter that accounts for reduced death rate in the treatment class
μ_h	Natural death rate for humans
μ_r	Natural death rate for rodents
ω	Rate at which individuals lose immunity

Table 2: Model Variables and description.

Variables	Description
S_h	Susceptible humans population
S_r	Susceptible rodents population
V_c	Covid-19 Vaccinated individuals
V_m	Monkeypox Vaccinated individuals
E_c^h	Exposed human Covid-19 Population
E_m^h	Exposed human Monkeypox Population
E_r	Exposed rodents population to Monkeypox
Q_c	Quarantined COVID-19 population
Q_m	Quarantined Monkeypox population
I_c^h	Infected COVID-19 Population
I_m^h	Infected Monkeypox Population
I_{cm}^h	Monkeypox and COVID-19 coinfected population
I_r	Infected rodents population
T_h	Treatment Class of humans
R_h	Individuals who have recovered from monkeypox, covid-19 and co- infections

3. Results and Analysis of the model

In this chapter, we analyze the mathematical model formulated in the preceding section to gain insights into the transmission dynamics of COVID-19 and Monkeypox co-infection within the human and rodent populations.

3.1. The Invariant Set

Theorem 3.1. *The solutions of model* (2.1) *remain feasible for all* $t > 0$ *provided that the initial conditions are taken from the invariant region*

$$D = D_1 \times D_2 \subset \mathbb{R}_+^{12} \times \mathbb{R}_+^3.$$

Proof:
To show that all feasible solutions of the system are uniformly bounded, we define the positively invariant sets D_1 and D_2 as follows:

$$D_1 = \left\{(S_h, V_c, V_m, E_c^h, E_m^h, Q_c, Q_m, I_c^h, I_m^h, I_{cm}^h, T_h, R_h) \in \mathbb{R}_+^{12} : S_h, V_c, V_m, E_c^h, E_m^h, Q_c, Q_m, I_c^h, I_m^h, I_{cm}^h, T_h, R_h > 0\right\},$$

and

$$D_2 = \left\{(S_r, E_r, I_r) \in \mathbb{R}_+^3 : S_r, E_r, I_r > 0\right\}.$$

Hence, any solution that starts in $D = D_1 \times D_2$ remains in D for all $t > 0$, establishing the feasibility of the model.

The total population of the human classes is
$N_h(t) = S_h(t) + V_c(t) + V_m(t) + E_c^h(t) + E_m^h(t) + Q_c(t) + Q_m(t) + I_m^h(t) + I_{cm}^h(t) + T_h(t) + R_r(t)$

The sum of the differentials is

$$\frac{dN_h}{dt} = \frac{dS_h}{dt} + \frac{dV_c}{dt} + \frac{dV_m}{dt} + \frac{dE_c^h}{dt} + \frac{dE_m^h}{dt} + \frac{dQ_c}{dt} + \frac{dQ_m}{dt} + \frac{dI_c^h}{dt} + \frac{dI_m^h}{dt} + \frac{dI_{cm}^h}{dt} + \frac{dT_h}{dt} + \frac{dR_h}{dt}$$

$$\frac{dN_h}{dt} = \Lambda_h - \mu_h N_h(t) - \delta_c I_c^h - \delta_m I_m^h - \eta\delta_c T_h,$$

$$\frac{dN_h}{dt} \leqslant \Lambda_h - \mu_h N_h(t) \tag{3.1}$$

Applying the integrating factor method to solve the differential equation (4.1), along with the given initial condition $t = 0$ and $N_h(t) = N_h(0)$

$$N_h(t) \leqslant \frac{\Lambda_h}{\mu_h}$$

Therefore,D_1 is said to be positively invariant under the model(2.1)
Similarly, the total population of the rodents classes is

$$N_r(t) \leqslant \frac{\Lambda_r}{\mu_r}$$

Therefore,D_1 and D_2 is said to be positively invariant under the model (2.1)
The analysis reveals that the overall human and rodent populations are limited above by the ratios $\frac{\Lambda_h}{\mu_h}$ and $\frac{\Lambda_r}{\mu_r}$, with μ_h and μ_r representing the natural death rates of humans and rodents, respectively. This constraint guarantees that the system's trajectories stay within a compact, positively invariant set that encompasses all biologically plausible solutions. It underscores the model's mathematical robustness and biological relevance, rendering it appropriate for both theoretical studies and practical simulations of COVID-19 and monkeypox co-infection dynamics.

3.2. Non-negativity of the solutions of model

To ensure that model (2.1) has epidemiological significance, it is essential to demonstrate that the solutions remain non-negative over time. This conclusion is derived from the theory presented below.

Theorem 3.2. *Given the initial states* $S_h(0) > 0$, $V_c(0) > 0$, $V_m(0) > 0$, $E_c^h(0) > 0$, $E_m^h(0) > 0$, $Q_c(0) > 0$, $Q_m(0) > 0$, $I_c^h(0) > 0$, $I_m^h(0) > 0$, $I_{cm}^h(0) > 0$, $T_h(0) > 0$, $R_h(0) > 0$, $S_r(0) > 0$, $E_r(0) > 0$, $I_r(0) > 0$. *Then the solutions* $(S_h(t), V_c(t), V_m(t), E_c^h(t), E_m^h(t), Q_c(t), Q_m(t), I_c^h(t), I_m^h(t), I_{cm}^h(t), T_h(t), R_h(t), S_r(t), E_r(t), I_r(t))$ *of model (3.8) are non-negative for all time* $t > 0$.

proof:
Let $t_1 = \sup\{t > 0 : S_h(t) > 0, V_c(t) > 0, V_m(t) > 0, E_c^h(t) > 0, E_m^h(t) > 0, Q_c(t) > 0, Q_m(t) > 0, I_c^h(t) > 0, I_m^h(t) > 0, I_{cm}^h(t) > 0, T_h(t) > 0, R_h(t) > 0, S_r(t) > 0, E_r(t) > 0, I_r(t) > 0 \in [0, t]\}$. From first equation of (2.1)

$$\frac{dS_h}{dt} = \Lambda_h + \psi_e V_e + \psi_m V_m + \omega R_h - (\theta_c + \theta_m + \lambda_e + \lambda_m + \mu_h) S_h. \tag{3.2}$$

Applying integrating factor, we have

$$S_h(t) = S_h(0)e^{-\int_0^t \mu(\tau)d\tau} + \int_0^t g(\tau)e^{-\int_\tau^t \mu(s)ds}d\tau > 0.$$

Hence, $S_h(t) > 0$ for all $t > 0$
Following the same procedure on $V_c(t), V_m(t), E_c^h(t), E_m^h(t), Q_c(t), Q_m(t), I_c^h(t), I_m^h(t), I_{cm}^h(t), T_h(t), R_h(t), S_r(t), E_r(t)$, and $I_r(t)$

Since all variables are expressed as integrals with positive integrands and positive initial conditions, each variable of model (2.1) remains positive for all $t > 0$.

3.3. Local Asymptotic Stability of the Disease-Free Equilibrium

The model (2.1) has a DFE, obtained by setting the left-hand side of the equations in the basic model (2.1) to zero, and this is given by

$$E_c^h = E_m^h = Q_c = Q_m = I_c^h = I_m^h = I_{cm}^h = T_h = R_h = E_r = I_r = 0, \lambda_c = \lambda_m = \lambda_r = 0$$

Thus, the disease-free equilibrium point of the co-infection model is

$$\mathcal{E}_0 = (S_h^*,\ V_c^*,\ V_m^*,\ 0,\ 0,\ 0,\ 0,\ 0,\ 0,\ 0,\ 0,\ 0,\ S_r^*,\ 0,\ 0)$$

Theorem 3.3. *The Disease free equilibrium (DFE) of the model* (2.1) *is locally asymptotically stable (LAS) whenever the basic reproduction number* $R_0 < 1$ *and unstable when* $R_0 > 1$.

proof:
The local asymptotic stability of the disease-free equilibrium will be established here using the Next Generation Operator Matrix based on our model (2.1), following the notation used by van den Driessche and Watmough (2002).The basic reproduction number of the COVID-19–Monkeypox co-infection model, denoted as R_0, is defined as the maximum of the basic reproduction numbers for COVID-19 transmission in the human population, R_0^c, Monkeypox transmission in the human population, R_0^m, and Monkeypox transmission in the rodent population, R_0^r.

$$R_0 = max.(R_0^c, R_0^m, R_0^r)$$

Utilizing the next-generation operator matrix approach, the basic reproduction number is determined as the dominant eigenvalue of the matrix FV^{-1}. Where, $f(x)$ matrix represents the rate at which new infections enter the disease compartment, while the $v(x)$ matrix reflects the rate of individual transfers both into and out of the disease compartment.
Let X be the set of the entire disease compartments. That is

$$\mathbf{x} = \left[E_c^h, E_m^h, Q_c, Q_m, I_c^h, I_m^h, I_{cm}^h, E_r, I_r\right]^T$$

Then our model can be written as

$$\frac{dX}{dt} = f(x) - v(x) \tag{3.3}$$

$$f = \begin{bmatrix} \lambda_c S_h \\ \lambda_m S_h \\ 0 \\ 0 \\ 0 \\ 0 \\ 0 \\ \lambda_r S_r \\ 0 \end{bmatrix}$$

$$\nu(x) = \begin{bmatrix} (\alpha_c^1 + \alpha_c^2 + \mu_h)E_c^h \\ (\alpha_m^1 + \alpha_m^2 + \mu_h)E_m^h \\ -\alpha_c^2 E_c^h + (\zeta_c \rho + \sigma + \mu_h)Q_c \\ -\alpha_m^2 E_m^h + (\zeta_m \rho + \mu_h)Q_m \\ -\alpha_c^1 E_c^h - \tau_m I_{cm}^h + (\gamma_c + \mu_h + \delta_c)I_c^h \\ -\alpha_m^1 E_m^h - \tau_c I_{cm}^h + (\gamma_m + \mu_h + \delta_m)I_m^h \\ -(\tau_m + \tau_c + \gamma_{cm} + \mu_h + \delta_{cm})I_{cm}^h \\ (\alpha_r + \mu_r)E_r \\ -\alpha_r E_r + \mu_r I_r \end{bmatrix}$$

$$F = \begin{bmatrix} 0 & 0 & 0 & 0 & \frac{\beta_c S_h^0}{N_h^0} & 0 & \frac{\beta_c S_h^0}{N_h^0} & 0 & 0 \\ 0 & 0 & 0 & 0 & 0 & \frac{\beta_m S_h^0}{N_h^0} & \frac{\beta_m S_h^0}{N_h^0} & 0 & \frac{\beta_1 S_h^0}{N_h^0} \\ 0 & 0 & 0 & 0 & 0 & 0 & 0 & 0 & 0 \\ 0 & 0 & 0 & 0 & 0 & 0 & 0 & 0 & 0 \\ 0 & 0 & 0 & 0 & 0 & 0 & 0 & 0 & 0 \\ 0 & 0 & 0 & 0 & 0 & 0 & 0 & 0 & 0 \\ 0 & 0 & 0 & 0 & 0 & 0 & 0 & 0 & 0 \\ 0 & 0 & 0 & 0 & 0 & 0 & 0 & 0 & \beta_r \\ 0 & 0 & 0 & 0 & 0 & 0 & 0 & 0 & 0 \end{bmatrix}$$

$$V = \begin{bmatrix} k_1 & 0 & 0 & 0 & 0 & 0 & 0 & 0 & 0 \\ 0 & k_2 & 0 & 0 & 0 & 0 & 0 & 0 & 0 \\ -\alpha_c^2 & 0 & k_3 & 0 & 0 & 0 & 0 & 0 & 0 \\ 0 & -\alpha_m^2 & 0 & k_4 & 0 & 0 & 0 & 0 & 0 \\ -\alpha_c^1 & 0 & 0 & 0 & k_5 & 0 & -\tau_m & 0 & 0 \\ 0 & -\alpha_m^1 & 0 & 0 & 0 & k_6 & -\tau_c & 0 & 0 \\ 0 & 0 & 0 & 0 & 0 & 0 & k_7 & 0 & 0 \\ 0 & 0 & 0 & 0 & 0 & 0 & 0 & k_8 & 0 \\ 0 & 0 & 0 & 0 & 0 & 0 & 0 & -\alpha_r & \mu_r \end{bmatrix}$$

where

$$V^{-1} = \begin{bmatrix} \frac{1}{k_1} & 0 & 0 & 0 & 0 & 0 & 0 & 0 & 0 \\ 0 & \frac{1}{k_2} & 0 & 0 & 0 & 0 & 0 & 0 & 0 \\ \frac{\alpha_c^2}{k_1 k_3} & 0 & \frac{1}{k_3} & 0 & 0 & 0 & 0 & 0 & 0 \\ 0 & \frac{\alpha_m^2}{k_2 k_4} & 0 & \frac{1}{k_4} & 0 & 0 & 0 & 0 & 0 \\ \frac{\alpha_c^1}{k_1 k_5} & 0 & 0 & 0 & \frac{1}{k_5} & 0 & 0 & 0 & 0 \\ 0 & \frac{\alpha_m^1}{k_2 k_6} & 0 & 0 & 0 & \frac{1}{k_6} & \frac{\tau_c}{k_6 k_7} & 0 & 0 \\ 0 & 0 & 0 & 0 & 0 & 0 & \frac{1}{k_7} & 0 & 0 \\ 0 & 0 & 0 & 0 & 0 & 0 & 0 & \frac{1}{k_8} & 0 \\ 0 & 0 & 0 & 0 & 0 & 0 & 0 & \frac{\alpha_r}{k_8 \mu_r} & \frac{1}{\mu_r} \end{bmatrix}$$

$$FV^{-1} = \begin{bmatrix} \frac{\beta_c \alpha_c^1 S_h^0}{N_h^0 k_1 k_5} & 0 & 0 & 0 & \frac{\beta_c S_h^0}{N_h^0 k_5} & 0 & \frac{\beta_c S_h^0}{N_h^0 k_7} & 0 & 0 \\ 0 & \frac{\beta_m \alpha_m^1 S_h^0}{N_h^0 k_2 k_6} & 0 & 0 & 0 & \frac{\beta_m S_h^0}{N_h^0 k_6} & \frac{\beta_m \tau_c S_h^0}{N_h^0 k_6 k_7} + \frac{\beta_m S_h^0}{N_h^0 k_7} & \frac{\beta_1 \alpha_r S_h^0}{N_h^0 k_8 \mu_r} & \frac{\beta_1 S_h^0}{N_h^0 \mu_r} \\ 0 & 0 & 0 & 0 & 0 & 0 & 0 & 0 & 0 \\ 0 & 0 & 0 & 0 & 0 & 0 & 0 & 0 & 0 \\ 0 & 0 & 0 & 0 & 0 & 0 & 0 & 0 & 0 \\ 0 & 0 & 0 & 0 & 0 & 0 & 0 & 0 & 0 \\ 0 & 0 & 0 & 0 & 0 & 0 & 0 & 0 & 0 \\ 0 & 0 & 0 & 0 & 0 & 0 & 0 & \frac{\beta_r \alpha_r}{k_8 \mu_r} & \frac{\beta_r}{\mu_r} \\ 0 & 0 & 0 & 0 & 0 & 0 & 0 & 0 & 0 \end{bmatrix}$$

The characteristic polynomial factors are as follows:

$$\det(M - \lambda I) = (-\lambda)^4 (M_{11} - \lambda)(M_{22} - \lambda)(M_{66} - \lambda)$$

where

$$M_{11} = \frac{\beta_c \alpha_c^1 S_h^0}{N_h^0 k_1 k_5}, \quad M_{22} = \frac{\beta_m \alpha_m^1 S_h^0}{N_h^0 k_2 k_6}, \quad M_{66} = \frac{\beta_r \alpha_r}{k_8 \mu_r}.$$

Thus, the eigenvalues are $\lambda = M_{11}, M_{22}, M_{66}$ (each with multiplicity 1) and $\lambda = 0$ (multiplicity 4)

The basic reproduction number R_0 is the spectral radius (dominant eigenvalue) of FV^{-1}. The dominant eigenvalues are:

$$R_0^c = \frac{\beta_c \alpha_c^1 S_h^0}{N_h^0 k_1 k_5} = \frac{\beta_c S_h^0 \alpha_c^1}{N_h^0 (\alpha_c^1 + \alpha_c^2 + \mu_h)(\gamma_c + \mu_h + \delta_c)}$$

$$R_0^m = \frac{\beta_m \alpha_m^1 S_h^0}{N_h^0 k_2 k_6} = \frac{\beta_m S_h^0 \alpha_m^1}{N_h^0 (\alpha_m^1 + \alpha_m^2 + \mu_h)(\gamma_m + \mu_h + \delta_m)}$$

$$R_0^r = \frac{\beta_r \alpha_r}{k_8 \mu_r} = \frac{\beta_r \alpha_r}{(\alpha_r + \mu_r)\mu_r}$$

we obtain:

$$R_0 = \max\left(\frac{\beta_c S_h^0 \alpha_c^1}{N_h^0 k_1 k_5}, \frac{\beta_m S_h^0 \alpha_m^1}{N_h^0 k_2 k_6}, \frac{\beta_r \alpha_r}{k_8 \mu_r} \right)$$

where

$$k_1 = \alpha_c^1 + \alpha_c^2 + \mu_h, \quad k_2 = \alpha_m^1 + \alpha_m^2 + \mu_h, \quad k_3 = \zeta_c\rho + \sigma + \mu_h, \quad k_4 = \zeta_m\rho + \mu_h,$$
$$k_5 = \gamma_c + \mu_h + \delta_c, \quad k_6 = \gamma_m + \mu_h + \delta_m, \quad k_7 = \tau_m + \tau_c + \gamma_{cm} + \mu_h + \delta_{cm}, \quad k_8 = \alpha_r + \mu_r.$$

Following [27], we make the claim below:

Lemma 3.4. *The disease free equilibrium (DFE) of the model* (2.1) *is locally asymptotically stable (LAS) whenever the basic reproduction number* $R_0 < 1$ *and unstable when* $R_0 > 1$

proof:
Here we prove lemma 6. The local stability of the (2.1) will be established using the linearization method. The jacobian matrix of the model (2.1) evaluated at disease free equilibrium

$$J(x_0) = \begin{pmatrix}
-(\theta_c+\theta_m+\mu_h) & \psi_c & \psi_m & 0 & 0 & 0 & 0 & 0 & 0 & 0 & 0 & \omega & 0 & 0 & 0 \\
\theta_c & -(\psi_c+\mu_h) & 0 & 0 & 0 & 0 & 0 & 0 & 0 & 0 & 0 & 0 & 0 & 0 & 0 \\
\theta_m & 0 & -(\psi_m+\mu_h) & 0 & 0 & 0 & 0 & 0 & 0 & 0 & 0 & 0 & 0 & 0 & 0 \\
0 & 0 & 0 & -G_1 & 0 & 0 & 0 & 0 & 0 & 0 & 0 & 0 & 0 & 0 & 0 \\
0 & 0 & 0 & 0 & -G_2 & 0 & 0 & 0 & 0 & 0 & 0 & 0 & 0 & 0 & 0 \\
0 & 0 & 0 & \alpha_c^2 & 0 & -G_3 & 0 & 0 & 0 & 0 & 0 & 0 & 0 & 0 & 0 \\
0 & 0 & 0 & 0 & \alpha_m^2 & 0 & -G_4 & 0 & 0 & 0 & 0 & 0 & 0 & 0 & 0 \\
0 & 0 & 0 & \alpha_c^1 & 0 & 0 & 0 & -G_5 & 0 & \tau_m & 0 & 0 & 0 & 0 & 0 \\
0 & 0 & 0 & 0 & \alpha_m^1 & 0 & 0 & 0 & -G_6 & \tau_c & 0 & 0 & 0 & 0 & 0 \\
0 & 0 & 0 & 0 & 0 & 0 & 0 & 0 & 0 & -G_7 & 0 & 0 & 0 & 0 & 0 \\
0 & 0 & 0 & 0 & 0 & \zeta_c\rho & \zeta_m\rho & \gamma_c & \gamma_m & \gamma_{cm} & -G_8 & 0 & 0 & 0 & 0 \\
0 & 0 & 0 & 0 & 0 & \sigma & 0 & 0 & 0 & 0 & \phi & -(\omega+\mu_h) & 0 & 0 & 0 \\
0 & 0 & 0 & 0 & 0 & 0 & 0 & 0 & 0 & 0 & 0 & 0 & -\mu_r & 0 & 0 \\
0 & 0 & 0 & 0 & 0 & 0 & 0 & 0 & 0 & 0 & 0 & 0 & 0 & -G_9 & 0 \\
0 & 0 & 0 & 0 & 0 & 0 & 0 & 0 & 0 & 0 & 0 & 0 & 0 & \alpha_r & -\mu_r
\end{pmatrix}.$$

where:

$$G_1 = \alpha_c^1 + \alpha_c^2 + \mu_h, \qquad G_2 = \alpha_m^1 + \alpha_m^2 + \mu_h,$$
$$G_3 = \zeta_c\rho + \sigma + \mu_h, \qquad G_4 = \zeta_m\rho + \mu_h,$$
$$G_5 = \pi\lambda_m + \gamma_c + \mu_h + \delta_c, \qquad G_6 = \pi\lambda_c + \gamma_m + \mu_h + \delta_m,$$
$$G_7 = \tau_m + \tau_c + \gamma_{cm} + \mu_h + \delta_{cm}, \qquad G_8 = \phi + \mu_h + \eta\delta_t,$$
$$G_9 = \alpha_r + \mu_r.$$

We must demonstrate that all the eigenvalues of the Jacobian matrix $J(x_0)$ are negative. The eleventh,thirteenth and last columns of $J(x_0)$ consist solely of diagonal elements, which give rise to the negative eigenvalues $-G_8$, $-\mu_r$ and $-\mu_r$.The remaining twelve (12) eigenvalue are obtained from the sub-matrix

$$J_1(x_0) = \begin{pmatrix} -(\theta_c+\theta_m+\mu_h) & \psi_c & \psi_m & 0 & 0 & 0 & 0 & 0 & 0 & 0 & \omega & 0 \\ \theta_c & -(\psi_c+\mu_h) & 0 & 0 & 0 & 0 & 0 & 0 & 0 & 0 & 0 & 0 \\ \theta_m & 0 & -(\psi_m+\mu_h) & 0 & 0 & 0 & 0 & 0 & 0 & 0 & 0 & 0 \\ 0 & 0 & 0 & -G_1 & 0 & 0 & 0 & 0 & 0 & 0 & 0 & 0 \\ 0 & 0 & 0 & 0 & -G_2 & 0 & 0 & 0 & 0 & 0 & 0 & 0 \\ 0 & 0 & 0 & \alpha_c^2 & 0 & -G_3 & 0 & 0 & 0 & 0 & 0 & 0 \\ 0 & 0 & 0 & 0 & \alpha_m^2 & 0 & -G_4 & 0 & 0 & 0 & 0 & 0 \\ 0 & 0 & 0 & \alpha_c^1 & 0 & 0 & 0 & -G_5 & 0 & \tau_m & 0 & 0 \\ 0 & 0 & 0 & 0 & \alpha_m^1 & 0 & 0 & 0 & -G_6 & \tau_c & 0 & 0 \\ 0 & 0 & 0 & 0 & 0 & 0 & 0 & 0 & 0 & -G_7 & 0 & 0 \\ 0 & 0 & 0 & 0 & 0 & \sigma & 0 & 0 & 0 & 0 & -(\omega+\mu_h) & 0 \\ 0 & 0 & 0 & 0 & 0 & 0 & 0 & 0 & 0 & 0 & 0 & -G_9 \end{pmatrix}.$$

Also, the eight, ninth and last column of $J_1(x_0)$ contains only the diagonal terms which forms the negative eigenvalues $-G_5$, $-G_6$ and $-G_9$. The remaining nine (9) eigenvalue are obtained from the sub-matrix

$$J_2(x_0) = \begin{pmatrix} -(\theta_c+\theta_m+\mu_h) & \psi_c & \psi_m & 0 & 0 & 0 & 0 & 0 & \omega \\ \theta_c & -(\psi_c+\mu_h) & 0 & 0 & 0 & 0 & 0 & 0 & 0 \\ \theta_m & 0 & -(\psi_m+\mu_h) & 0 & 0 & 0 & 0 & 0 & 0 \\ 0 & 0 & 0 & -G_1 & 0 & 0 & 0 & 0 & 0 \\ 0 & 0 & 0 & 0 & -G_2 & 0 & 0 & 0 & 0 \\ 0 & 0 & 0 & \alpha_c^2 & 0 & -G_3 & 0 & 0 & 0 \\ 0 & 0 & 0 & 0 & \alpha_m^2 & 0 & -G_4 & 0 & 0 \\ 0 & 0 & 0 & 0 & 0 & 0 & 0 & -G_7 & 0 \\ 0 & 0 & 0 & 0 & 0 & \sigma & 0 & 0 & -(\omega+\mu_h) \end{pmatrix}$$

Also, the eight column of $J_2(x_0)$ contains only the diagonal term which forms the negative eigenvalues$-G_7$.The remaining eight (8) eigenvalue are obtained from the sub-matrix

$$J_3(x_0) = \begin{pmatrix} -(\theta_c+\theta_m+\mu_h) & \psi_c & \psi_m & 0 & 0 & 0 & 0 & \omega \\ \theta_c & -(\psi_c+\mu_h) & 0 & 0 & 0 & 0 & 0 & 0 \\ \theta_m & 0 & -(\psi_m+\mu_h) & 0 & 0 & 0 & 0 & 0 \\ 0 & 0 & 0 & -G_1 & 0 & 0 & 0 & 0 \\ 0 & 0 & 0 & 0 & -G_2 & 0 & 0 & 0 \\ 0 & 0 & 0 & \alpha_c^2 & 0 & -G_3 & 0 & 0 \\ 0 & 0 & 0 & 0 & \alpha_m^2 & 0 & -G_4 & 0 \\ 0 & 0 & 0 & 0 & 0 & \sigma & 0 & -(\omega+\mu_h) \end{pmatrix}.$$

The matrix $J_3(x_0)$ can be partitioned into block-diagonal and block-triangular components for easier calculation of the eigenvalues.
After solving partitioned matrices, we found out that all eigenvalues of $J_3(x_0)$ have negative real parts (under the condition $R_0 < 1$), we conclude that the DFE, $\mathcal{E}_\mathcal{O}$ is locally asymptotically stable.

3.4. Global Asymptotic Stability of the Disease-Free Equilibrium of the Model

To examine the global asymptotic stability of the disease-free equilibrium in the model (2.1), we apply the method developed by Castillo-Chavez and Song as outlined in [21]. Let $X = (S_h, V_c, V_m, R_h, S_r) \in R^5_+$ denote uninfected population and let $Z = (E^h_c, E^h_m, Q_c, Q_m, I^h_c, I^h_m, I^h_{cm}, T_h, E_r, I_r) \in R^{10}_+$ denote infected population
We write the equations of uninfected class as

$$\frac{dX}{dt} = F(X, Z) \tag{3.4}$$

Also we write the equation of infected class as

$$\frac{dZ}{dt} = G(X, Z) \tag{3.5}$$

Let $\mathcal{E}_0 = (X^*, 0)$ represents the disease-free equilibrium point of the model (2.1)

The system (2.1) is GAS if it satisfies the following conditions:

1. H_1: $\frac{dX}{dt} = F(X^*, 0), X^*$ is globally asymptotically stable.
2. H_2: $\frac{dZ}{dt} = D_Z G(X^*, 0)Z - \bar{G}(X, Z)$,

$\bar{G}(X, Z) \geqslant 0$ for all $(X, Z) \in D$

where $D_Z G(X^*, 0)Z$ represents an M-matrix (characterized by non-negative diagonal elements, also serving as the Jacobian of $G(X, Z)$ and computed for $(X^*, 0)$, the ensuing theorem is applicable, provided the system meets the aforementioned criterion.

Theorem 3.5. *The disease free equilibrium point $\mathcal{E}_O = (X^*, 0)$ is globally asymptotically stable if $R_O \leqslant 1$ and H_1, H_2 are satisfied.*

Proof. Let, □

$$F(X,Z) = \begin{bmatrix} \Lambda_h + \psi_c V_c + \psi_m V_m + \omega R_h - (\theta_c + \theta_m + \lambda_c + \lambda_m + \mu_h) S_h \\ \theta_c S_h - (\psi_c + \mu_h) V_c \\ \theta_m S_h - (\psi_m + \mu_h) V_m \\ \phi_m T_h + \sigma Q_c - (\chi\lambda_c + \omega + \mu_h) R_h \\ \Lambda_r - (\lambda_r + \mu_r) S_r \end{bmatrix}$$

$$G(X,Z) = \begin{bmatrix} \lambda_c S_h - G_1 E^h_c \\ \lambda_m S_h - G_2 E^h_m \\ \alpha^2_c E^h_c - G_3 Q_c \\ \alpha^2_m E^h_m - G_4 Q_m \\ \alpha^1_c E^h_c + \chi\lambda_c R_h + \tau_m I^h_{cm} - G_5 I^h_c \\ \alpha^1_m E^h_m + \tau_c I^h_{cm} - G_6 I^h_m \\ \pi\lambda_m I^h_c + \pi\lambda_c I^h_m - G_7 I^h_{cm} \\ \zeta_c \rho Q_c + \zeta_m \rho Q_m + \gamma_c I^h_c + \gamma_m I^h_m + \gamma_{cm} I^h_{cm} - G_8 T_h \\ \lambda_r S_r - G_9 E_r = 0 \\ \alpha_r E_r - \mu_r I_r = 0 \end{bmatrix}$$

$$D_Z G(X^*,0)Z = \begin{bmatrix} -G_1 E_c^h + \beta_c I_c^h + \beta_c I_{cm}^h \\ -G_2 E_m^h + \beta_m I_m^h + \beta_m I_{cm}^h + \beta_r I_m^r \\ \alpha_c^2 E_c^h - G_3 Q_c \\ \alpha_m^2 E_m^h - G_4 Q_m \\ \alpha_c^1 E_c^h + \chi\lambda_c R_h + \tau_m I_{cm}^h - G_5 I_c^h \\ \alpha_m^1 E_m^h + \tau_c I_{cm}^h - G_6 I_m^h \\ \pi\lambda_m I_c^h + \pi\lambda_c I_m^h - G_7 I_{cm}^h \\ \zeta_c \rho Q_c + \zeta_m \rho Q_m + \gamma_c I_c^h + \gamma_m I_m^h + \gamma_{cm} I_{cm}^h - G_8 T_h \\ -G_9 E_r + \beta_r I_r \\ \alpha_r E_r - \mu_r I_r \end{bmatrix}$$

At the disease free equilibrium point,

$$H_1 : \frac{dS_h}{dt} = \Lambda_h + \psi_c V_c + \psi_m V_m - (\theta_c + \theta_m + \mu_h) S_h$$

$$\frac{dV_c}{dt} = \theta_c S_h - (\psi_c + \mu_h) V_c$$

$$\frac{dV_m}{dt} = \theta_m S_h - (\psi_m + \mu_h) V_m$$

$$\frac{dR_h}{dt} = 0$$

$$\frac{dS_r}{dt} = \Lambda_r - \mu_r S_r$$

$$H_2 \colon \bar{G}(X,Z) = D_Z G(X^*,0)Z - \bar{G}(X,Z),$$

$$G(X,Z) = \begin{bmatrix} (\beta_c I_c^h + \beta_c I_{cm}^h)(1 - \frac{S_h}{N_h}) \\ (\beta_m I_m^h + \beta_m I_{cm}^h)(1 - \frac{S_h}{N_h}) \\ 0 \\ 0 \\ 0 \\ 0 \\ 0 \\ 0 \\ \beta_r I_r (1 - \frac{S_r}{N_r}) \\ 0 \end{bmatrix}$$

Remark 3.6. Clearly, $1 \geqslant \frac{S_h}{N_h}$ and $1 \geqslant \frac{S_r}{N_r}$ this implies that $\bar{G}(X,Z) \geqslant 0$ Consequently, the disease-free equilibrium (DFE) of the COVID-19 and monkeypox co-infection model is globally asymptotically stable. This indicates that, irrespective of the initial number of infected individuals in the population, the diseases will eventually be eradicated as long as the basic reproduction number R_0 remains below one. Thus, the finding that the DFE maintains global asymptotic stability under the condition of $R < 1$ reinforces the feasibility of completely eliminating both COVID-19 and monkeypox from the population, provided there is no reintroduction of the viruses. This underscores the critical need for ongoing intervention strategies and highlights the importance of consistently vaccinating individuals to establish robust immunity against these diseases.

3.5. Global Stability Analysis For Endemic Equilibrium

Theorem 3.7. *The endemic equilibrium (EE) of the model* (2.1) *is globally asymptotically stable whenever* $R_0 > 1$

To establish global stability of the EE, we construct a Lyapunov function of the form:

$$\mathcal{L} = \sum_{i=1}^{9} C_i \left(X_i - X_i^* - X_i^* \ln \frac{X_i}{X_i^*} \right),$$

where X_i represents the compartments
$(S_h, V_c, V_m, E_c^h, E_m^h, Q_c, Q_m, I_c^h, I_m^h, I_{cm}^h, T_h, S_r, E_r, I_r)$ and $C_i > 0$ are constants to be determined.

Consider the nonlinear Lyapunov function

$$\begin{aligned}
\mathcal{L} = C_1 \Big[& S_h - S_h^* - S_h^* \ln\left(\frac{S_h}{S_h^*}\right) + E_c^h - E_c^{h*} - E_c^{h*} \ln\left(\frac{E_c^h}{E_c^{h*}}\right) \\
& + E_m^h - E_m^{h*} - E_m^{h*} \ln\left(\frac{E_m^h}{E_m^{h*}}\right) + V_c - V_c^* - V_c^* \ln\left(\frac{V_c}{V_c^*}\right) \\
& + V_m - V_m^* - V_m^* \ln\left(\frac{V_m}{V_m^*}\right) \Big] \\
& + C_2 \left[Q_c - Q_c^* - Q_c^* \ln\left(\frac{Q_c}{Q_c^*}\right) \right] + C_3 \left[Q_m - Q_m^* - Q_m^* \ln\left(\frac{Q_m}{Q_m^*}\right) \right] \\
& + C_4 \left[I_c^h - I_c^{h*} - I_c^{h*} \ln\left(\frac{I_c^h}{I_c^{h*}}\right) \right] + C_5 \left[I_m^h - I_m^{h*} - I_m^{h*} \ln\left(\frac{I_m^h}{I_m^{h*}}\right) \right] \\
& + C_6 \left[I_{cm}^h - I_{cm}^{h*} - I_{cm}^{h*} \ln\left(\frac{I_{cm}^h}{I_{cm}^{h*}}\right) \right] + C_7 \left[T_h - T_h^* - T_h^* \ln\left(\frac{T_h}{T_h^*}\right) \right] \\
& + C_8 \left[S_r - S_r^* - S_r^* \ln\left(\frac{S_r}{S_r^*}\right) + E_r - E_r^* - E_r^* \ln\left(\frac{E_r}{E_r^*}\right) \right] \\
& + C_9 \left[I_r - I_r^* - I_r^* \ln\left(\frac{I_r}{I_r^*}\right) \right].
\end{aligned} \tag{3.6}$$

Differentiating (3.6), we have

$$\begin{aligned}
\dot{\mathcal{L}} = C_1 \Big[& \dot{S_h} - \frac{S_h^*}{S_h}\dot{S_h} + \dot{E_c^h} - \frac{E_c^{h*}}{E_c^h}\dot{E_c^h} + \dot{E_m^h} - \frac{E_m^{h*}}{E_m^h}\dot{E_m^h} + \dot{V_c} - \frac{V_c^*}{V_c}\dot{V_c} + \dot{V_m} - \frac{V_m^*}{V_m}\dot{V_m} \Big] \\
& + C_2 \left[\dot{Q_c} - \frac{Q_c^*}{Q_c}\dot{Q_c} \right] + C_3 \left[\dot{Q_m} - \frac{Q_m^*}{Q_m}\dot{Q_m} \right] + C_4 \left[\dot{I_c^h} - \frac{I_c^{h*}}{I_c^h}\dot{I_c^h} \right] \\
& + C_5 \left[\dot{I_m^h} - \frac{I_m^{h*}}{I_m^h}\dot{I_m^h} \right] + C_6 \left[\dot{I_{cm}^h} - \frac{I_{cm}^{h*}}{I_{cm}^h}\dot{I_{cm}^h} \right] + C_7 \left[\dot{T_h} - \frac{T_h^*}{T_h}\dot{T_h} \right] \\
& + C_8 \left[\dot{S_r} - \frac{S_r^*}{S_r}\dot{S_r} + \dot{E_r} - \frac{E_r^*}{E_r}\dot{E_r} \right] + C_9 \left[\dot{I_r} - \frac{I_r^*}{I_r}\dot{I_r} \right].
\end{aligned}$$

$$\mathcal{L} = C_1\left[\left(1-\frac{S_h^*}{S_h}\right)\dot{S_h}+\left(1-\frac{E_c^{h*}}{E_c^h}\right)\dot{E_c^h}+\left(1-\frac{E_m^{h*}}{E_m^h}\right)\dot{E_m^h}++\left(1-\frac{V_c^*}{V_c}\right)\dot{V_c}+C_3\left(1-\frac{V_m^*}{V_m}\right)\dot{V_m}\right]$$
$$C_2\left[\left(1-\frac{Q^*c}{Q_c}\right)\dot{Q_c}\right]+C_3\left[\left(1-\frac{Q_m^*}{Q_m}\right)\dot{Q_m}\right]+C_4\left[\left(1-\frac{I_c^{h*}}{I_c^h}\right)\dot{I_c^h}\right]+C_5\left[\left(1-\frac{I_m^{h*}}{I_m^h}\right)\dot{I_m^h}\right]$$
$$+C_6\left[\left(1-\frac{I_{cm}^{h*}}{I_{cm}^h}\right)\dot{I_{cm}^h}\right]+C_7\left[\left(1-\frac{T_h^*}{T_h}\right)\dot{T_h}\right]+C_8\left[\left(1-\frac{S_r^*}{S_r}\right)\dot{S_r}+\left(1-\frac{E_r^*}{E_r}\right)\dot{E_r}\right]$$
$$+C_9\left[\left(1-\frac{I_r^*}{I_r}\right)\dot{I_r}\right] \tag{3.7}$$

Where upper dot represents the derivatives of the model (2.1) with respect to time t. Hence, substituting the equations of the model (2.1) in (3.7), we have

$$\mathcal{L} = C_1\left[\left(1-\frac{S_h^*}{S_h}\right)\left(\Lambda_h+\psi_c V_c+\psi_m V_m+\omega R_h-\theta_c S_h-\theta_m S_h-\lambda_c S_h-\lambda_m S_h-\mu_h S_h\right)\right.$$
$$+\left(1-\frac{E_c^*}{E_c}\right)\left(\lambda_c S_h-G_1 E_c^h\right)+\left(1-\frac{E_m^*}{E_m}\right)\left(\lambda_m S_h-G_2 E_m^h\right)$$
$$+\left(1-\frac{V_c^*}{V_c}\right)\left(\theta_c S_h-\psi_c V_c-\mu_h V_c\right)$$
$$\left.+\left(1-\frac{V_m^*}{V_m}\right)\left(\theta_m S_h-\psi_m V_m-\mu_h V_m\right)\right]$$
$$+C_2\left[\left(1-\frac{Q_c^*}{Q_c}\right)\left(\alpha_c^2 E_c^h-G_3 Q_c\right)\right]+C_3\left[\left(1-\frac{Q_m^*}{Q_m}\right)\left(\alpha_m^2 E_m^h-G_4 Q_m\right)\right]$$
$$+C_4\left[\left(1-\frac{I_c^{h*}}{I_c^h}\right)\left(\alpha_c^1 E_c^h+\chi\lambda_c R_h+\tau_m I_{cm}^h-G_5 I_c^h\right)\right]+C_5\left[\left(1-\frac{I_m^{h*}}{I_m^h}\right)\left(\alpha_m^1 E_m^h+\tau_c I_{cm}^h-G_6 I_m^h\right)\right]$$
$$+C_6\left[\left(1-\frac{I_{cm}^{h*}}{I_{cm}^h}\right)\left(\pi\lambda_m I_c^h+\pi\lambda_c I_m^h-G_7 I_{cm}^h\right)\right]$$
$$+C_7\left[\left(1-\frac{T_h^*}{T_h}\right)\left(\zeta_c\rho Q_c+\zeta_m\rho Q_m+\gamma_c I_c^h+\gamma_m I_m^h+\gamma_{cm} I_{cm}^h-G_8 T_h\right)\right]$$
$$+C_8\left[\left(1-\frac{S_r^*}{S_r}\right)\left(\Lambda_r-\lambda_r S_r-\mu_r S_r+\left(1-\frac{E_r^*}{E_r}\right)\left(\lambda_r S_r-G_9 E_r\right)\right]\right.$$
$$+C_9\left[\left(1-\frac{I_r^*}{I_r}\right)\left(\alpha_r E_r-\mu_r I_r\right)\right] \tag{3.8}$$

At steady state of (3.8), we have

$$\Lambda_h = \theta_c S_h^* + \theta_m S_h^* + \lambda_c S_h^* + \lambda_m S_h^* + \mu_h S_h^* - \psi_c V_c^* - \psi_m V_m^* - \omega R_h^*, \quad \Lambda_r = \lambda_r S_r^* + \mu_r S_r^*,$$

$$G_1 = \frac{\lambda_c S_h^*}{E_c^{h*}}, \quad G_2 = \frac{\lambda_m S_h^*}{E_m^{h*}}, \quad G_3 = \frac{\alpha_c^2 E_c^{h*}}{Q_c^*}, \quad G_4 = \frac{\alpha_m^2 E_m^{h*}}{Q_m^*},$$

$$G_5 = \frac{\alpha_c^1 E_c^{h*} + \chi\lambda_c R_h^* + \tau_m I_{cm}^{h*}}{I_c^{h*}}, \quad G_6 = \frac{\alpha_m^1 E_m^{h*} + \tau_c I_{cm}^{h*}}{I_m^{h*}}, \quad G_7 = \frac{\pi\lambda_m I_c^{h*} + \pi\lambda_c I_m^{h*}}{I_{cm}^{h*}},$$

$$G_8 = \frac{\zeta_c \rho Q_c^* + \zeta_m \rho Q_m^* + \gamma_c I_c^{h*} + \gamma_m I_m^{h*} + \gamma_{cm} I_{cm}^{h*}}{T_h^*}, \quad G_9 = \frac{\lambda_r S_r^*}{E_r^*}$$

then we substitute the value of Λ_h and Λ_r in (3.8)

$$\begin{aligned}
\mathcal{L} = C_1 &\Bigg[\left(1 - \frac{S_h^*}{S_h}\right) \left(\theta_c S_h^* + \theta_m S_h^* + \lambda_c S_h^* + \lambda_m S_h^* + \mu_h S_h^* - \psi_c V_c^* - \psi_m V_m^* - \omega R_h^* + \psi_c V_c + \psi_m V_m \right. \\
&\left. + \omega R_h - \theta_c S_h - \theta_m S_h - \lambda_c S_h - \lambda_m S_h - \mu_h S_h \right) \\
&+ \left(1 - \frac{E_c^*}{E_c}\right) \left(\lambda_c S_h - G_1 E_c^h\right) + \left(1 - \frac{E_m^*}{E_m}\right) \left(\lambda_m S_h - G_2 E_m^h\right) \\
&+ \left(1 - \frac{V_c^*}{V_c}\right) \left(\theta_c S_h - \psi_c V_c - \mu_h V_c\right) + \left(1 - \frac{V_m^*}{V_m}\right) \left(\theta_m S_h - \psi_m V_m - \mu_h V_m\right) \Bigg] \\
&+ C_2 \left[\left(1 - \frac{Q_c^*}{Q_c}\right) \left(\alpha_c^2 E_c^h - G_3 Q_c\right) \right] + C_3 \left[\left(1 - \frac{Q_m^*}{Q_m}\right) \left(\alpha_m^2 E_m^h - G_4 Q_m\right) \right] \\
&+ C_4 \left[\left(1 - \frac{I_c^{h*}}{I_c^h}\right) \left(\alpha_c^1 E_c^h + \chi\lambda_c R_h + \tau_m I_{cm}^h - G_5 I_c^h\right) \right] + C_5 \left[\left(1 - \frac{I_m^{h*}}{I_m^h}\right) \left(\alpha_m^1 E_m^h + \tau_c I_{cm}^h - G_6 I_m^h\right) \right] \\
&+ C_6 \left[\left(1 - \frac{I_{cm}^{h*}}{I_{cm}^h}\right) \left(\pi\lambda_m I_c^h + \pi\lambda_c I_m^h - G_7 I_{cm}^h\right) \right] \\
&+ C_7 \left[\left(1 - \frac{T_h^*}{T_h}\right) \left(\zeta_c \rho Q_c + \zeta_m \rho Q_m + \gamma_c I_c^h + \gamma_m I_m^h + \gamma_{cm} I_{cm}^h - G_8 T_h\right) \right] \\
&+ C_8 \left[\left(1 - \frac{S_r^*}{S_r}\right) \left(\Lambda_r - \lambda_r S_r - \mu_r S_r + \left(1 - \frac{E_r^*}{E_r}\right) \left(\lambda_r S_r - G_9 E_r\right) \right] \right. \\
&+ C_9 \left[\left(1 - \frac{I_r^*}{I_r}\right) \left(\alpha_r E_r - \mu_r I_r\right) \right]
\end{aligned} \tag{3.9}$$

After solving for the lyapunov constants, we have

$$C_1 = -\frac{\alpha_m^1}{G_2 G_6 \lambda_m}, \quad C_2 = 0, \quad C_3 = 0, \quad C_4 = -\frac{G_1 \alpha_m^1}{G_2 G_6 \alpha_c^1 \lambda_m}, C_5 = -\frac{G_2 \alpha_c^1}{G_1 G_5 \alpha_m^1 \lambda_c}, \quad C_6 = -\frac{G_1 G_5 \alpha_m^1}{G_2 G_6 \pi \alpha_c^1 \lambda_m^2}$$

Now, substituting the values of $C_1, C_2, C_3, C_4, C_5, C_6, C_7, C_8$,and C_9 in equation (3.9),we have

$$\begin{aligned}\mathcal{L} = &-\frac{\alpha_m^1}{G_2G_6\lambda_m}\Big[\theta_c S_h^* + \theta_m S_h^* + \lambda_c S_h^* + \lambda_m S_h^* + \mu_h S_h^* - \psi_c V_c^* - \psi_m V_m^* - \omega R_h^* + \psi_c V_c + \psi_m V_c \\ &+ \omega R_h - \mu_h S_h - \frac{\theta_c S_h^{*2}}{S_h} - \frac{\theta_m S_h^{*2}}{S_h} - \frac{\lambda_c S_h^{*2}}{S_h} - \frac{\lambda_m S_h^{*2}}{S_h} - \frac{\mu_h S_h^{*2}}{S_h} + \frac{\psi_c V_c^* S_h^*}{S_h} + \frac{\psi_m V_m^* S_h^*}{S_h} \\ &+ \frac{\omega R_h^* S_h^*}{S_h} - \frac{\psi_c V_c S_h^*}{S_h} - \frac{\psi_m V_m S_h^*}{S_h} - \frac{\omega R_h S_h^*}{S_h} + \theta_c S_h^* + \theta_m S_h^* + \lambda_c S_h^* + \lambda_m S_h^* + \mu_h S_h^* \\ &- G_1 E_c^h - \frac{\lambda_c S_h E_c^*}{E_c^h} + G_1 E_c^{h*} - \psi_c V_c - \mu_h V_c - \frac{\theta_c S_h V_c^*}{V_c} + \psi_c V_c^* + \mu_h V_c^* - G_2 E_m^h \\ &- \frac{\lambda_m S_h E_m^*}{E_m^h} + G_2 E_m^{h*} - \psi_m V_m - \mu_h V_m - \frac{\theta_m S_h V_m^*}{V_m} + \psi_m V_m^* - + \mu_h V_m^*\Big] \\ &- \frac{G_1\alpha_m^1}{G_2G_6\alpha_c^1\lambda_m}\Big[\alpha_c^1 E_c^h + \chi\lambda_c R_h + \tau_m I_{cm}^h - G_5 I_c^h - \frac{\alpha_c^1 E_c^h I_c^{h*}}{I_c^h} - \frac{\chi\lambda_c R_h I_c^{h*}}{I_c^h} - \frac{\tau_m I_{cm}^h I_c^{h*}}{I_c^h} + G_5 I_c^{h*}\Big] \\ &- \frac{G_2\alpha_c^1}{G_1G_5\alpha_m^1\lambda_c}\Big[\alpha_m^1 E_m^h + \tau_c I_{cm}^h - G_6 I_m^h - \frac{\alpha_m^1 E_m^h I_m^{h*}}{I_m^h} - \frac{\tau_c I_{cm}^h I_m^{h*}}{I_m^h} + G_6 I_m^{h*}\Big] \\ &- \frac{G_1G_5\alpha_m^1}{G_2G_6\pi\alpha_c^1\lambda_m^2}\Big[\pi\lambda_m I_c^h + \pi\lambda_c I_m^h - G_7 I_{cm}^h - \frac{\pi\lambda_m I_c^h I_{cm}^{h*}}{I_{cm}^h} - \frac{\pi\lambda_c I_m^h I_{cm}^{h*}}{I_{cm}^h} + G_7 I_{cm}^h\Big]\end{aligned} \tag{3.10}$$

From (3.10) we collect all the terms with dot-stars in the infected classes including all $\mu_h S_h^*, \mu_r S_r^*$ and $\mu_h S_h, \mu_r S_r$

$$\begin{aligned}\mathcal{L} = &-\frac{\alpha_m^1}{G_2G_6\lambda_m}\Big[G_1 E_c^{h*} + G_2 E_c^{h*} - \frac{\lambda_c S_h E_c^{h*}}{E_c^h} - \frac{\lambda_m S_h E_m^{h*}}{E_m^h}\Big] - \frac{\alpha_m^1}{G_2G_6\lambda_m}\Big[2\mu_h S_h^* - \mu_h S_h - \frac{\mu_h S_h^{*2}}{S_h}\Big] \\ &- \frac{G_1\alpha_m^1}{G_2G_6\alpha_c^1\lambda_m}\Big[G_5 I_c^{h*} - \frac{\alpha_c^1 E_c^h I_c^{h*}}{I_c^h} - \frac{\chi\lambda_c R_h I_c^{h*}}{I_c^h} - \frac{\tau_m I_{cm}^h I_c^{h*}}{I_c^h}\Big] \\ &- \frac{G_2\alpha_c^1}{G_1G_5\alpha_m^1\lambda_c}\Big[G_6 I_m^{h*} - \frac{\alpha_m^1 E_m^h I_m^{h*}}{I_m^h} - \frac{\tau_c I_{cm}^h I_m^{h*}}{I_m^h}\Big] \\ &- \frac{G_1G_5\alpha_m^1}{G_2G_6\pi\alpha_c^1\lambda_m^2}\Big[G_7 I_{cm}^h - \frac{\pi\lambda_m I_c^h I_{cm}^{h*}}{I_{cm}^h} - \frac{\pi\lambda_c I_m^h I_{cm}^{h*}}{I_{cm}^h}\Big]\end{aligned} \tag{3.11}$$

Hence, substitute the steady state of G_1, G_2, G_5, G_6 and G_7 in (3.11)

$$\mathcal{L} = -\frac{\alpha_m^1 E_m^{h*} I_m^{h*}}{\lambda_m^2 S_h^*(\alpha_m^1 E_m^{h*} + \tau_c I_{cm}^h)}\left(\lambda_c S_h^* + \lambda_m S_h^* - \frac{\lambda_c S_h E_c^{h*}}{E_c^h} - \frac{\lambda_m S_h E_m^{h*}}{E_m^h}\right) - \frac{\alpha_m^1 \mu_h E_m^{h*} I_m^{h*}}{\lambda_m^2(\alpha_m^1 E_m^{h*} + \tau_c I_{cm}^h)}$$
$$\left(2 - \frac{S_h}{S_h^*} - \frac{S_h^*}{S_h}\right) - \frac{\lambda_c \alpha_m^1 E_m^{h*} I_m^{h*}}{\lambda_m^2 \alpha_c^1 E_c^{h*}(\alpha_m^1 E_m^{h*} + \tau_c I_{cm}^{h*})}$$
$$\times \left(\alpha_c^1 E_c^{h*} + \chi\lambda_c R_h^* + \tau_m I_{cm}^{h*} - \frac{\alpha_c^1 E_c^h I_c^{h*}}{I_c^h} - \frac{\chi\lambda_c R_h I_c^{h*}}{I_c^h} - \frac{\tau_m I_{cm}^h I_c^{h*}}{I_c^h}\right)$$
$$- \frac{\lambda_c^2 \alpha_m^1 E_m^{h*}(\alpha_c^1 E_c^{h*} + \chi\lambda_c R_h^* + \tau_m I_{cm}^{h*})}{\lambda_m E_c^{h*} I_c^{h*}}\left(\alpha_m^1 E_m^{h*} + \tau_c I_{cm}^{h*} - \frac{\alpha_m^1 E_m^h I_m^{h*}}{I_m^h} - \frac{\tau_c I_{cm}^h I_m^{h*}}{I_m^h}\right)$$
$$- \frac{\lambda_c \alpha_m^1 E_m^{h*} I_m^{h*}(\alpha_c^1 E_c^{h*} + \chi\lambda_c R_h^* + \tau_m I_{cm}^{h*})}{\lambda_m^3 \alpha_c^1 \pi E_c^{h*} I_c^{h*}(\alpha_m^1 E_m^{h*} + \tau_c I_{cm}^{h*})}\left(\pi\lambda_m I_c^{h*} + \pi\lambda_c I_m^{h*} - \frac{\pi\lambda_m I_c^h I_{cm}^{h*}}{I_{cm}^h} - \frac{\pi\lambda_c I_m^h I_{cm}^{h*}}{I_{cm}^h}\right) \tag{3.12}$$

As the arithmetic mean is greater than the geometric mean, the following inequalities hold:

$$\left(2 - \frac{S_h^*}{S_h} - \frac{S_h}{S_h^*}\right) \leqslant 0, \quad \left(\lambda_c S_h^* + \lambda_m S_h^* - \frac{\lambda_c S_h E_c^{h*}}{E_c^h} - \frac{\lambda_m S_h E_m^{h*}}{E_m^h}\right) \leqslant 0,$$
$$\left(\alpha_c^1 E_c^{h*} + \chi\lambda_c R_h^* + \tau_m I_{cm}^{h*} - \frac{\alpha_c^1 E_c^h I_c^{h*}}{I_c^h} - \frac{\chi\lambda_c R_h I_c^{h*}}{I_c^h} - \frac{\tau_m I_{cm}^h I_c^{h*}}{I_c^h}\right) \leqslant 0,$$
$$\left(\alpha_m^1 E_m^{h*} + \tau_c I_{cm}^{h*} - \frac{\alpha_m^1 E_m^h I_m^{h*}}{I_m^h} - \frac{\tau_c I_{cm}^h I_m^{h*}}{I_m^h}\right) \leqslant 0,$$
$$\left(\pi\lambda_m I_c^{h*} + \pi\lambda_c I_m^{h*} - \frac{\pi\lambda_m I_c^h I_{cm}^{h*}}{I_{cm}^h} - \frac{\pi\lambda_c I_m^h I_{cm}^{h*}}{I_{cm}^h}\right) \leqslant 0,$$

Hence, $\dot{\mathcal{L}} \leqslant 0$ for $\bar{R}_0 > 1$. Therefore, $\mathcal{L}$ is a Lyapunov function in D and by LaSalle Invariance Principle it concluded that the GAS of EEP is globally asymptotically stable for $\bar{R}_0 > 1$. The global stability analysis of the endemic equilibrium within the co-infection model offers important insights into the long-term dynamics of the system affected by both COVID-19 and monkeypox.

3.6. Modification Parameters for Mortality Reduction in the Treated Individuals

This analysis examines the modification parameter η that accounts for reduced mortality rates in treated individuals within the COVID-19 and Monkeypox co-infection model. The parameter η plays a crucial role in quantifying the effectiveness of therapeutic interventions.

The treatment compartment T_h evolves according to:

$$\frac{dT_h}{dt} = \zeta_c \rho Q_c + \zeta_m \rho Q_m + \gamma_c I_c^h + \gamma_m I_m^h + \gamma_{cm} I_{cm}^h - (\phi + \mu_h + \eta\delta_t)T_h \tag{3.13}$$

- $\eta \in [0, 1]$ acts as a **reduction factor** for mortality in T_h.
- δ_t: Baseline disease-induced mortality rate
- ϕ: Recovery rate from treatment

- μ_h: Natural mortality rate

The outflow term from the treatment compartment can be decomposed as:

$$\text{Outflow} = \underbrace{\phi T_h}_{\text{Recovery}} + \underbrace{\mu_h T_h}_{\text{Natural Death}} + \underbrace{\eta\delta_t T_h}_{\text{Disease-Induced Death}}$$

At equilibrium, setting $\frac{dT_h}{dt} = 0$:

$$T_h^* = \frac{\zeta_c \rho Q_c^* + \zeta_m \rho Q_m^* + \gamma_c I_c^{h*} + \gamma_m I_m^{h*} + \gamma_{cm} I_{cm}^{h*}}{\phi + \mu_h + \eta\delta_t}$$

The dependence on η shows that lower values increase the equilibrium treatment population.

The partial derivatives reveal parameter sensitivity:

$$\frac{\partial T_h^*}{\partial \eta} = -\frac{\delta_t T_h^*}{(\phi + \mu_h + \eta\delta_t)} < 0$$
$$\frac{\partial D_T}{\partial \eta} = \delta_t T_h^* > 0$$
$$\frac{\partial R_h^*}{\partial \eta} = -\frac{\phi\delta_t T_h^*}{(\phi + \mu_h + \eta\delta_t)(\chi\lambda_c + \omega + \mu_h)} < 0$$

We provide the graphs from our analysis along with their interpretations. The model's parameter values and state variables are based on data regarding the Florida population and outbreak information from the CDC, WHO, and the Florida Health Department.

Table 3: Key epidemiological parameters of the co-infection model with their estimated values and sources

Parameter	**Value / Range**	**Source**
Λ_h	5.8×10^2/day	[22]
ζ_c	0.05–0.1/day	[23]
ζ_m	0.02–0.05/day	[24]
γ_c	0.05–0.1/day	[23]
γ_m	0.02–0.05/day	[24]
γ_{cm}	0.01–0.03/day	Assumed
ϕ	0.05–0.1/day	[24]
μ_h	3.9×10^{-5}/day	[26]

The modification parameter η serves as a critical interface between mathematical modeling and clinical reality in the co-infection dynamics of COVID-19 and Monkeypox. Our analysis reveals several key insights in figures below.

Figure 2, 3 and 4 bellow presents three graphs: Treatment Compartment Dynamics, Variation of η, and Final Treated Population vs η. The first graph, Treatment Compartment Dynamics, illustrates how the trajectory of the treatment population evolves based on treatment effectiveness. The T_h curve peaks higher and maintains an elevated level

throughout the year. This indicates that effective treatment (low η) corresponds to a lower death rate in the T_h compartment. With fewer deaths, individuals remain in the treatment compartment for longer periods, either until natural recovery or through treatment, resulting in an accumulation of patients in treatment.

The second graph, Variation of η, tracks the populations of individuals who are quarantined (Q_c, Q_m), infected with either of two diseases (I_c, I_m), co-infected $(I_c m)$, or undergoing treatment (T_h). The primary variable assessed in this model is η, which represents the effectiveness of treatment in reducing disease-related mortality. When η ranges from 0.0 to 0.3, treatment is considered highly effective, significantly lowering the death rate for patients in the T_h compartment. Conversely, when η is between 0.8 and 1.0, treatment is less effective, resulting in minimal reduction of the death rate for patients in the T_h compartment. The graph captures the baseline dynamics of the treatment population and associated deaths over one year. Initially, there is a substantial influx of patients entering treatment from the pools of quarantined and infected individuals $(Q_c, I_c, etc.)$. This inflow rate significantly surpasses the outflow, which consists of recovery and death. The treatment population peaks and subsequently declines as the initial reservoirs of infected and quarantined individuals deplete (as indicated in the simplified ODEs for $\frac{dI_c}{dt}$, etc., which are all negative). Over time, the inflow into T_h slows, and the curve begins to flatten as the system nears a steady state where the new cases entering treatment balance the recoveries and deaths of those already being treated. While the curve shows a steady rise, reflecting ongoing mortality within the treatment compartment, the rate of new deaths accumulating decreases over time. This is a direct result of the declining T_h population, with fewer individuals in treatment at risk of dying.

The final graph, which compares the Final Treated Population and η, quantifies the relationship between treatment effectiveness and the long-term strain on the healthcare system. There is a pronounced, non-linear decrease in the final size of the treatment population as η increases. Higher final T_h values at low η indicate that effective treatment results in a persistent population of survivors who require medical care. Conversely, lower final T_h values at high η signify a concerning trend, reflecting that ineffective treatment yields a smaller treatment population, as fewer patients survive long enough to necessitate ongoing care. This graph highlights a significant trade-off: enhancing treatment efficacy (lowering η) will inevitably intensify the long-term demand for treatment facilities and resources. Policymakers must plan accordingly to accommodate this increased capacity to harness the life-saving benefits of improved treatments. The objective is to manage a larger population of living patients, rather than a smaller one resulting from high mortality. In summary, these three graphs provide a comprehensive illustration of the interaction between treatment efficacy and disease dynamics.

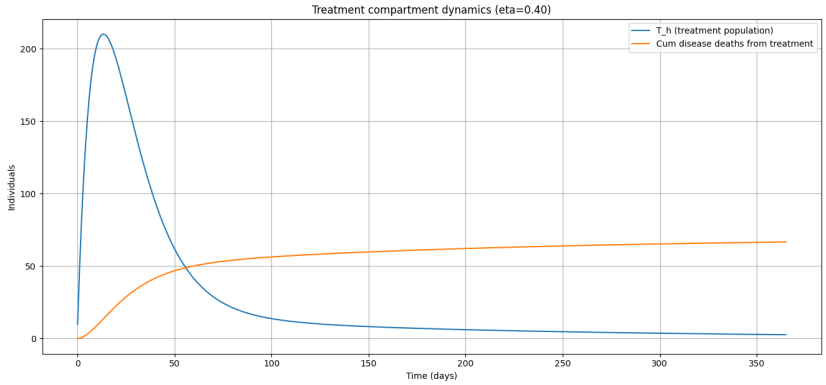

Figure 2: Treatment Compartment Dynamics

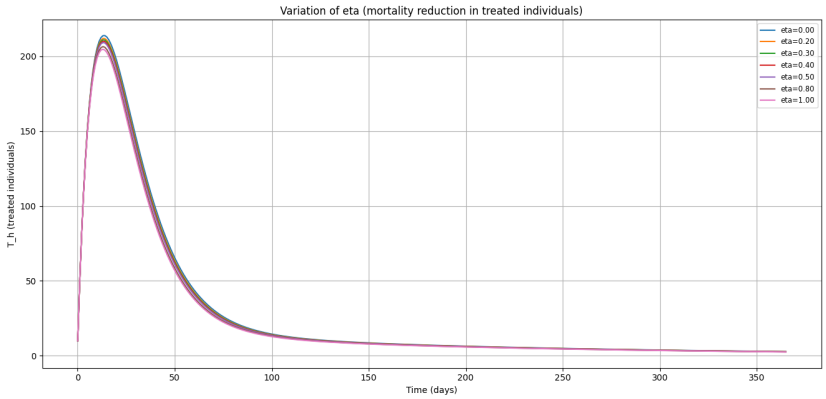

Figure 3: Variation of η

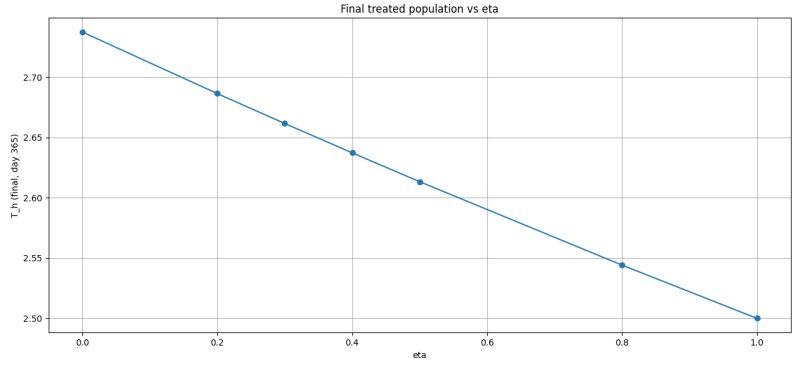

Figure 4: Final Treated Population vs η

3.7. Impacts of COVID-19 on Monkeypox

We examine both direct and indirect pathways through which COVID-19 affects Monkeypox transmission and progression. To Examine the Monkeypox Infection Pathway

$$\lambda_m = \frac{\beta_1 I_r + \beta_m (I_m^h + I_{cm}^h)}{N_h}$$

Here, I_{cm} (co-infected individuals) contribute to Monkeypox transmission, implying that:

1. COVID-19-infected individuals who become co-infected also drive Monkeypox transmission.
2. The presence of COVID-19 enhances the infectious pool for Monkeypox via I_{cm}

This term shows COVID-19 indirectly increases Monkeypox transmission by increasing the number of co-infected individuals.
Co-infection Dynamics (Monkeypox-only infectious class:)

$$\frac{dI_m^h}{dt} = \alpha_m^1 E_m^h + \tau_c I_{cm}^h - (\pi\lambda_c + \gamma_m + \mu_h + \delta_m) I_m^h$$

Co-infected class dynamics:

$$\frac{dI_{cm}^h}{dt} = \pi\lambda_m I_c^h + \pi\lambda_c I_m^h - (\tau_m + \tau_c + \gamma_{cm} + \mu_h + \delta_{cm}) I_{cm}^h$$

The term $\pi\lambda_m I_c^h$ shows that COVID-19-infected individuals (in can develop Monkeypox upon exposure — leading to co-infection. This increases the burden on Monkeypox dynamics, as co-infected individuals I_{cm} are more infectious (affecting λ_m) and possibly harder to treat. Therefore, COVID-19 increases the reservoir for Monkeypox transmission.

Original Monkeypox reproduction number (without considering COVID-19 impact):

$$R_0^m = \frac{\alpha_m^1 \beta_m S_h^O}{k_2 k_6 N_h^0}$$

However, due to co-infection, the effective force of infection becomes:

$$\lambda_m = \frac{\beta_1 I_r + \beta_m (I_m^h + I_{cm}^h)}{N_h}$$

This reflects how I_{cm} (driven by COVID-19 dynamics) enhances Monkeypox transmission, thus raising the effective reproduction number above the baseline R_0^m.

COVID-19 impacts Monkeypox by:

1. Increasing co-infection rates, thereby enlarging the Monkeypox-infectious pool.
2. Raising the effective force of infection λ_m and effective reproduction number R_0
3. Complicating treatment and public health efforts, potentially reducing the efficacy of Monkeypox-specific interventions.

Table 4: Summary of COVID-19 Impact on Monkeypox

Pathway	**Description**	**Impact**
Co-infection Term I_{cm}	COVID-19 triggers co-infection	Boosts Monkeypox spread
Force of Infection λ_m	I_{cm} adds to spread	Increases λ_m force
Reproduction Number	R_0 rises with co-infection	Harder Monkeypox control
Treatment Competition	T_h treats both	Resources stretched, γ_m drops
Public Health Burden	Increases case complexity	Diagnosis and care harder

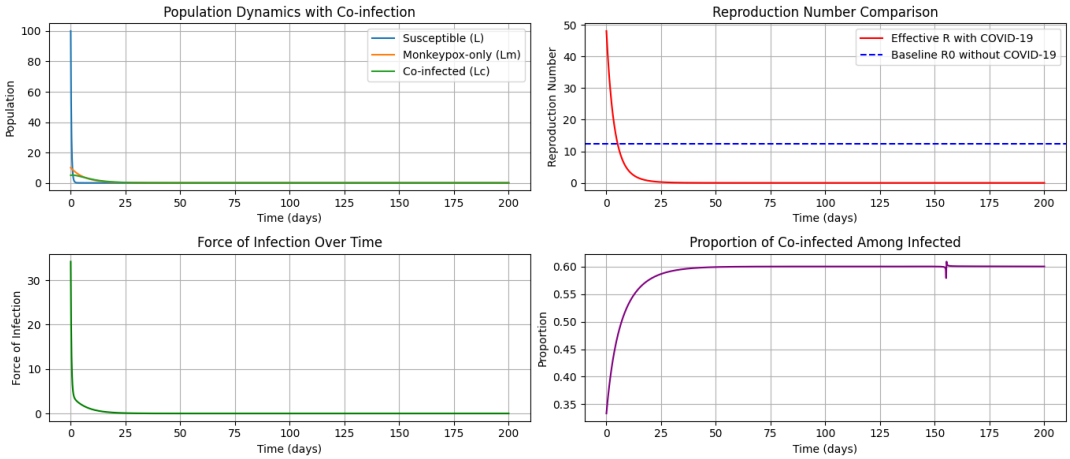

Figure 5: Treatment Compartment Dynamics

Our results highlight that co-infection, reduced immune response due to prior COVID-19 infection, and shifts in vaccination and quarantine strategies can amplify Monkeypox transmission. This interaction indicates that controlling COVID-19 also aids in the containment of Monkeypox, highlighting the need for integrated management strategies in cases of co-infection. In Figure 5 below, the first graph illustrates the temporal changes in the populations of susceptible individuals, those infected solely with Monkeypox, and co-infected individuals. The second graph contrasts the baseline reproduction number R0 (not accounting for the impact of COVID-19) with the effective reproduction number that reflects the influence of co-infection with COVID-19. The third graph depicts the variations in the force of infection (λ_m) over time, accounting for both direct and indirect transmission routes. The fourth graph monitors the proportion of total infections that consist of co-infections. Overall, these findings suggest that COVID-19 elevates the effective reproduction number for Monkeypox. Additionally, the presence of co-infected individuals amplifies the force of infection. Over time, a considerable percentage of infections evolve into co-infections.

3.8. Biological Features of the Model

The model describes the transmission dynamics of COVID-19 and Monkeypox within a human population while incorporating important intervention strategies such as vaccination, quarantine, treatment, and reinfection. The population is divided into epidemiological compartments representing susceptible individuals, individuals infected with COVID-19, individuals infected with Monkeypox, co-infected individuals, quarantined individuals, and individuals undergoing treatment.

Susceptible individuals become infected through effective contact with infectious individuals, which is represented in the model through the forces of infection. Quarantine reduces the spread of infection by isolating exposed individuals, while treatment improves recovery and reduces disease-induced mortality. The modification parameter η represents the effectiveness of treatment in reducing mortality among treated individuals. Lower values of η correspond to more effective treatment and higher survival rates.

The model also captures the interaction between COVID-19 and Monkeypox through a co-infection class. Biologically, individuals infected with one disease may become more susceptible to the other due to weakened immune response. Vaccination reduces the number of susceptible individuals, while reinfection accounts for the possibility of waning immunity.

Overall, the model reflects key biological mechanisms governing the spread and control of COVID-19 and Monkeypox and highlights the importance of combined intervention strategies in reducing co-infection dynamics.

4. Summary and Conclusion

4.1. Summary

Based on compartmental modeling concepts, this research develops a deterministic compartmental model reflecting co-infections involving COVID-19 and Monkeypox, with focus on interventions associated with vaccination, quarantine, treatment, and reinfections. A compartmental model breaks down the human populations into various compartments.

From the mathematical analysis, there exist some crucial properties of the model. First, it can be seen that the region of interest and positivity conditions imply epidemiologically meaningful solutions. Next, the disease-free equilibrium solution and local stability have been obtained. The basic reproduction number R_0 value can be determined via the next generation matrix. The global asymptotic stability of the disease-free equilibrium solution using the Castillo-Chavez and Song method and global stability analysis via a Lyapunov function for an endemic equilibrium solution have been shown.

A parameter η, measuring the treatment efficacy against mortality rate among treated individuals, is included. Simulation experiments show how η affects treatment outcomes. A low value of η implies low mortality rate and an accumulating number of treated individuals. However, a large value of η implies an ineffective treatment and a small final number of treated individuals.

Subsequent analysis focuses on the impact of COVID-19 on the Monkeypox transmission dynamics. The findings demonstrate that co-infections, an immunosuppressed state caused by COVID-19 infections, and changes to control measures result in an increase

in the reproduction number and force of infection for Monkeypox. A large number of incidences progress to co-infections.

In general, it can be said that the results have shown the intertwined relationship between COVID-19 and Monkeypox and have implications for comprehensive immunization and quarantine and treatment strategies against co-circulation.

4.2. Conclusion

In this study, a deterministic mathematical model was developed to investigate the co-infection dynamics of COVID-19 and Monkeypox by incorporating vaccination, quarantine, treatment, and reinfection mechanisms. The analytical results established that the model is mathematically well-posed through the derivation of invariant region and the proof of non-negativity of solutions. The disease-free equilibrium (DFE) and the associated basic reproduction number R_0 were obtained, and their stability properties were rigorously analyzed. The local stability of the DFE was established using the next-generation matrix approach, while global stability was proven using the Castillo–Chavez and Song method. Furthermore, the global stability of the endemic equilibrium was demonstrated using a suitable Lyapunov function.

Numerical simulations provided important insights into the biological behavior of the system and the effects of intervention strategies. The graphical results showed that the modification parameter η, which represents the effectiveness of treatment in reducing mortality among treated individuals, plays a crucial role in determining the dynamics of the treatment compartment T_h. The treatment dynamics indicate that when treatment is highly effective (small η), more infected individuals survive and remain in treatment for longer periods, leading to a larger treated population over time. Conversely, when treatment effectiveness decreases (large η), mortality increases and fewer individuals remain in treatment. This highlights an important public health implication that improving treatment effectiveness reduces mortality but may increase the long-term demand on healthcare resources.

The simulation results further revealed the epidemiological interaction between COVID-19 and Monkeypox. The figures demonstrate that the presence of co-infected individuals increases the effective reproduction number and amplifies the force of infection of Monkeypox. As a result, COVID-19 infection can indirectly facilitate the spread of Monkeypox, leading to a higher proportion of co-infections in the population. These results emphasize that disease interactions can significantly influence transmission dynamics and must be considered when designing control strategies.

Overall, the findings suggest that integrated intervention strategies combining vaccination, effective quarantine measures, and improved treatment are essential for controlling the co-infection of COVID-19 and Monkeypox. Strengthening treatment effectiveness reduces mortality, while coordinated control of COVID-19 transmission can also help limit the spread of Monkeypox. These results provide useful insights for policymakers and public health authorities in designing comprehensive strategies to reduce the burden of co-infection and improve epidemic preparedness.

Area of Further Study

This research has provided valuable insights into the co-infection dynamics of COVID-19 and Monkeypox. The ongoing second phase of this study focuses on the numerical aspects of the co-infection, specifically examining control strategies, sensitivity analysis, and simulations regarding the effects of vaccination rates, vaccine failure, quarantine, and treatment control. However, several areas remain open for further investigation.

1. **Incorporation of Heterogeneous Populations:**
   The current model assumes uniform mixing within human and rodent populations. Future research could build upon this by incorporating age-structured, spatially diverse, or network-based populations to better reflect actual transmission dynamics (Brauer, Castillo-Chavez, and Feng, (2019)).
2. **Stochastic Modeling and Uncertainty Analysis:**
   Given that the spread of infectious diseases is inherently random, a stochastic version of this model would aid in quantifying variability and outbreak probabilities. This approach could be combined with an uncertainty analysis of parameters to more effectively reflect real-world unpredictability (Inyama, and Iheonu (2015): Fadikar, Stevens, Collier, Toh, Morozova, Hotton, Ozik, and others.(2024)).
3. **Integration of Behavioral and Social Dynamics:**
   Human behaviors, including adherence to quarantine, reluctance to receive vaccines, and perceptions of risk, have a substantial impact on the outcomes of epidemics. Future models need to include the dynamics of these behaviors and the feedback mechanisms that affect the effectiveness of interventions(Zhang, Fang, Liu, and others. (2025)).
4. **Variant and Strain Evolution:**
   The existing framework does not consider the emergence of new viral strains or variants. Expanding the model to include mutation and strain competition would enhance its relevance in rapidly changing epidemic situations(Ahumada, Ledesma-Araujo, Gordillo, and Marín, (2022)).
5. **Economic and Cost-Effectiveness Analysis:**
   Future research may combine the epidemiological model with economic frameworks to assess the cost-effectiveness of interventions such as vaccination, revaccination, and dual treatments. This approach would offer direct guidance for policymakers facing resource limitations (Ruiz, Sherratt, Ekwueme, Adepoju, and Abbas (2023); Akinyemi etal (2023)).
6. **Real-Time Data Assimilation and Predictive Modeling:**
   Integrating the model with real epidemiological data streams through parameter estimation and machine learning techniques would improve predictive accuracy. This would render the framework a practical decision-support tool for managing outbreaks(Gibson, Fox, Javan, Ptak, Ibrahim, Lachmann, and Meyers, (2025)).
7. **Extension to Multi-Pathogen Interactions:**
   This study concentrated on COVID-19 and Monkeypox, but future research could investigate three-way interactions, such as those involving COVID-19, Monkeypox, and HIV, or examine the interactions between viral and bacterial infections, thus

expanding the focus of co-infection research (Liu, Rakhmanina, Yang, and Bukrinsky (2024)).

References

[1] Markus Hoffmann, Hannah Kleine-Weber, Simon Schroeder, Nadine Krüger, Tanja Herrler, Sandra Erichsen, Tobias S. Schiergens, and others (2020). *SARS-CoV-2 cell entry depends on ACE2 and TMPRSS2 and is blocked by a clinically proven protease inhibitor*. Cell, 181(2), 271–280.

[2] Kristian G. Andersen, Andrew Rambaut, W. Ian Lipkin, Edward C. Holmes, and Robert F. Garry (2020).*The proximal origin of SARS-CoV-2*. Nature Medicine, 26, 450–452.

[3] Andrew Hill (2013). *The ecology and evolution of zoonotic diseases*. Proceedings of the National Academy of Sciences (PNAS), 110(20), 8399–8400.

[4] Ying Liu, Albert A. Gayle, Annelies Wilder-Smith, and Joacim Rocklöv (2020). *The reproductive number of COVID-19 is higher compared to SARS coronavirus*.Journal of Travel Medicine, 27(2).

[5] Wei-jie Guan, Zheng-yi Ni, Yu Hu, Wen-hua Liang, Chun-quan Ou, Jian-xing He, Lei Liu, Hong Shan, Chun-liang Lei,and others (2020). *Clinical characteristics of coronavirus disease 2019 in China*. New England Journal of Medicine, 382, 1708–1720.

[6] Joost Wiersinga, Andrew Rhodes, Allen C. Cheng, Sharon J. Peacock, and Hallie C. Prescott (2020). *Pathophysiology, transmission, diagnosis, and treatment of COVID-19: A review*. JAMA, 324(8), 782–793.

[7] Ladnyj, I. D. Ziegler, P. and Kima, E. (1972).*A human infection caused by monkeypox virus in Basankusu Territory, Democratic Republic of the Congo*.Bulletin of the World Health Organization, 46, 593–597.

[8] Anne M. Likos, Suzanne A. Sammons, Victoria A. Olson, Andrea M. Frace, Yvonne Li, Margarita Olsen-Rasmussen, William Davidson, John A. G. Smith, Richard L. Regnery, and Inger K. Damon (2005). *A tale of two clades: Monkeypox viruses*. Journal of General Virology, 86, 2661–2672.

[9] Centers for Disease Control and Prevention (2022).*Monkeypox: Epidemiology, transmission, and outbreaks*.CDC.gov.

[10] Mary G. Reynolds, Kazunori Yorita, Michael J. Kuehnert, William B. Davidson, Victoria A. Huhn, John A. Holman, and Inger K. Damon (2006). *Clinical manifestations of human monkeypox influenced by route of infection*. Journal of Infectious Diseases, 194(6), 773–780.

[11] Kurt D. Reed, Joseph W. Melski, Mark B. Graham, John M. Regnery, Michael J. Sotir, Maureen Wegner, David L. Kazmierczak, and others (2004).*The detection of monkeypox in the United States*. New England Journal of Medicine, 350, 342–350.

[12] Moritz U. G. Kraemer, Houriiyah Tegally, David M. Pigott, Bernard M. Greenwood, Oliver G. Pybus, and Samuel V. Scarpino (2022).*The 2022 global mpox outbreak: Epidemiology and implications*. The Lancet Infectious Diseases, 22, 1112–1121.

[13] World Health Organization (2022a). *Multi-country monkeypox outbreak: Situation update*.WHO.int.

[14] Víctor A. Benites-Zapata, Jhony A. Ulloque-Badaracco, Percy L. Alarcon-Braga, Diego Hernandez-Bustamante, and Carlos A. Rodriguez-Morales (2023).*Clinical challenges in co-infection with COVID-19 and Monkeypox*.Travel Medicine and Infectious Disease, 52 .

[15] Eze, F. C., Iwa, L. L., Adam, U. M., and Audu, A. M. (2025).A mathematical analysis of tuberculosis transmission using a two-age group compartmental model.*Journal of Mathematical Analysis and Modeling*, 6(2), 100–126.https://doi.org/10.48185/jmam.v6i2.1657.

[16] Nicolas Vabret, Gregory J. Britton, Conor Gruber, Samarth Hegde, Jonghyeon Kim, Maria Kuksin, Roman Levantovsky, Laura Malle, Javier Moreira, Marisa D. Park, Anna Pia, Esther Racanelli, Thomas J. Smith, Olivia S. Zaid, and Miriam Merad (2020).*Immunology of COVID-19*.Immunity, 52(6), 910–941.

[17] Anupam Patel, Julia Bilinska, Joanna C. Tam, Matthew Da Silva Filho, and Christina Pagel (2022). *Vaccination and prevention strategies for Monkeypox and COVID-19 co-circulation*. BMJ Global Health, 7(11).

[18] Akin Oyewale Yinka-Ogunleye, Obafemi Aruna, Mohammed Dalhat, Babatunde Ogoina, Ifedayo McCollum, Peter Disu, Godwin Mamadu, Maryam Ahmed, Adesola Adeoye, Chukwuma Chukwuogo, Adesina M. Saleh, Patrick Nguku, Emmanuel Idris, and Oyewale Tomori (2019).
Outbreak of human monkeypox in Nigeria in 2017–18: A clinical and epidemiological report. The Lancet Infectious Diseases, 19(8), 872–879.

[19] Eze, F. C., Idowu, K. O., Adam, U. M., and Olofin, D. O. (2025).Mathematical modelling of the endemic phase of COVID-19 infection considering vaccination breakthrough, revaccination and reinfection.*International Journal of Applied Mathematics and Modelling*, 8(2), 148-180.

[20] Acheneje, G.O., Omale, D., Otokolo, W., & Bolaji, B. (2024). *Modeling the transmission dynamics of the co-infection of COVID-19 and Monkeypox diseases with optimal control strategies and cost–benefit analysis*. Franklin Open Journal 8, 100130

[21] Castillo-Chavez, C. and Song, B. (2004).Dynamical models of tuberculosis and their applications. *Mathematical Biosciences and Engineering*,2,361–404.http://dx.doi.org/10.1007/s10598-023-09564-7.

[22] United States Census Bureau (2020). National population estimates. *U.S. Census Bureau*.

[23] Centers for Disease Control and Prevention (2020). COVID-19 control and prevention. *CDC*.

[24] World Health Organization (2022). Monkeypox: Public health advice for gay, bisexual and other men who have sex with men. *World Health Organization*, Geneva, Switzerland. Available at: https://www.who.int/publications/i/item/WHO-MPX-Guidance-2022.1

[25] Eze, F. C., and Uwaezuoke, M. U. (2025).Age-structured deterministic model for the dynamics of Hepatitis B virus in Nigeria incorporating vertical and horizontal transmission.*International Journal of Mathematical and Applied Modelling*, 8 (2), 212-251.

[26] Elizabeth Arias and Jiaquan Xu (2021). United States life tables. *National Vital Statistics Reports*, 70(19):1–64.

[27] van den Driessche, P. and Watmough, J. (2002).Reproduction numbers and sub-threshold endemic equilibria for compartmental models of disease transmission.*Mathematical Biosciences*, 180(1–2), 29–48.https://doi.org/10.1016/S0025-5564(02)00108-6.

[28] Shah, K., Ahmad, S., Ullah, A., and Abdeljawad, T. (2024).Study of chronic myeloid leukemia with T-cell under fractal-fractional order model. *Open Physics*, 22(1), 20240032. https://doi.org/10.1515/phys-2024-0032.

[29] Shah, K., Rehman, K. U., Abdalla, B., Abdeljawad, T., and Shatanawi, W. (2025). Using neural network and fractals fractional analysis to predict the eye disease infection caused by conjunctivitis virus.*Fractals*, 33(6), 2540204. https://doi.org/10.1142/S0218348X25402042.

[30] Shah, K., Ullah, A., Abdeljawad, T., and Shatanawi, W. (2024).Analytical study of a modified-ABC fractional order breast cancer model.*Journal of Applied Mathematics and Computing*, 70(4), 3685–3716. https://doi.org/10.1007/s12190-023-01942-2.

[31] Shah, K., Rehman, K. U., Abdeljawad, T., and Shatanawi, W. (2025).Modeling virus mutation dynamics using piecewise fractional derivatives.*European Journal of Pure and Applied Mathematics*, 18(2), 6053–6068.

[32] Alzahrani, F., Alqahtani, F., and Shah, K. (2021).Mathematical modeling and forecasting of COVID-19 in Saudi Arabia under fractal-fractional derivative in Caputo sense with power-law.*Axioms*, 10(12), 941. https://doi.org/10.3390/axioms10120941.

[33] Khan, M. A., Atangana, A., and Baleanu, D. (2024). Conformable fractional-order modeling and analysis of HIV/AIDS transmission dynamics.*International Journal of Differential Equations*, 2024, Article ID 1234567. https://doi.org/10.1155/2024/1234567.

[34] Jeelani, M. B., Alnahdi, A. S., Abdo, M. S., Almalahi, M. A., Alharthi, N. H., and Shah, K. (2023).A generalized fractional order model for CoV-2 with vaccination effect using real data.*Fractals*, 31(4), 2340042.https://doi.org/10.1142/S0218348X2340042X.

[35] Alqudah, M. A., Shah, K., Mofarreh, F., and Abdeljawad, T. (2025).Mathematical modeling of psychological disease by using artificial intelligence tools.*Fractals*, 34(1), 2550101.https://doi.org/10.1142/S0218348X25501014.

[36] Obi, V. O., Eze, F., and Nwajeri, K. U. (2025).Transmission dynamics of cholera disease using fractional-order model.*Journal of Mathematical Analysis and Modeling*, 6(3), 84–112.

[37] Eze, F. C., Nwadibia, A. I., Inyama, S. C., Omame, A., and Godwin, E. C. (2020).Analysis of the transmission dynamics for Zika virus with nonlinear force of infections. *Journal of Mathematical Sciences & Computational Mathematics*, 1(2), 119–165. https://doi.org/10.15864/jmscm.1201.

[38] Nwadibia, A. I., Eze, F. C., Inyama, S. C., Nse, C. A., Omame, A., and Mbachu, H. I. (2018).Mathematical model of the transmission dynamics of genital elephantiasis (lymphatic filariasis).*Mathematical Theory and Modeling*, 8(4), 71–113.